European Journal of Medicinal Chemistry 109 (2016) 59–74

Contents lists available at ScienceDirect

European Journal of Medicinal Chemistry

journal homepage: http://www.elsevier.com/locate/ejmech

Research paper

Design and synthesis of pyrrolobenzodiazepine-gallic hybrid agents as p53-dependent and -independent apoptogenic signaling in melanoma cells

Yu-Wei Chou [a], Gopal Chandru Senadi [b], Chung-Yu Chen [c], Kung-Kai Kuo [d], Ying-Ting Lin [a], Jeh-Jeng Wang [b], Jia-Hau Lee [b], Ya-Ching Wang [a], Wan-Ping Hu [a, *]

[a] Department of Biotechnology, Kaohsiung Medical University, Kaohsiung, Taiwan
[b] Department of Medicinal and Applied Chemistry, Kaohsiung Medical University, Kaohsiung, Taiwan
[c] School of Pharmacy, Kaohsiung Medical University, Kaohsiung, Taiwan
[d] Department of Surgery, School of Medicine, Kaohsiung Medical University, Taiwan

ARTICLE INFO

Article history:
Received 12 June 2015
Received in revised form
11 September 2015
Accepted 20 December 2015
Available online 23 December 2015

Keywords:
Pyrrolobenzodiazepine
Mitochondria
Gallic acid
Antitumor
Free radical
Melanoma

ABSTRACT

A new class of pyrrolo[2,1-*c*][1,4]benzodiazepine-Gallic hybrid agents (PBD-GA) conjugated through alkyl spacers has been designed and synthesized. The combination of these two core pharmacophores with modification in the C-8 position of the PBD ring with alkyl spacers afforded oxygen-tethered compounds **5a**–**5d** and amide-tethered analogues **11a**–**11d** with improved anticancer activity for two melanoma cell lines, A375 and RPMI7951, differing in their p53 status. The agents **5a**–**5d** were cytotoxic in melanoma compared to agents **11a**–**11d**. In particular, compounds **5b** and **5c** were found to possess the most potent activity compared with other hybrid agents and were proved with the help of quantitative structure activity relationship studies (QSAR). These PBD conjugates caused S phase arrest for the A375 cell line via increased reactive oxygen species (ROS) generation, deoxyribonucleic acid (DNA) damage, ataxia telangiectasia mutated (ATM)/ATM-Rad3-related (ATR) and checkpoint kinases 1 (Chk1) activation. Moreover, the PBD-GA induced A375 apoptotic cell death followed through p53 (ATM downstream target) increase, B-cell leukemia-xL (Bcl-xL) and mitochondrial membrane potential ($\Delta\Psi_{mt}$) decrease, cytochrome *c* release, and caspase-3/Poly Adp Ribose Polymerase (PARP) cleavage. On the other hand, mutant p53 RPMI7951 cell death occurred by PBD-GA-mediated mitochondria- and caspase-dependent pathways via lysosomal membrane permeabilization (LMP), but not through p53 signaling. Finally, compound **5b** was shown to reduce murine melanoma size in a mouse model. These results suggest that the PBD-GA could be used as a useful chemotherapeutic agent in melanoma with activated p53 or mutant p53.

1. Introduction

Pyrrolo[2,1-c][1,4]-benzodiazepines (PBDs) cores are some of the most potent naturally occurring antibiotics from the family of *Streptomyces* species. These compounds are known to exhibit antitumor activity via sequence-selective binding to the B-form of DNA and inhibiting the synthesis of nucleic acid [1]. However, only a few DNA-interactive agents have been discovered to bind DNA with high sequence selectivity [2,3]. Hence, the discovery of novel small-molecule drug candidates is still an essential area of research.

In this context, for the last few years our research group has focused on developing new PBD conjugates and evaluating their binding ability. We have also reported an efficient synthesis of DC-81 (Fig. 1A) with an overall yield of 35% over 6 steps (67% yield based on the recovered starting material at the fifth step) [4]. In general, DC-81 and indole carboxylate core molecules are commonly used as medicinal compounds such as antimitotic drugs [5,6]. Based on this fact, in 2006, we synthesized DC-81 hybrids linked with indole carboxylates and the preliminary in vivo tests

Abbreviations used: PBD-GA, pyrrolo[2,1-*c*] [1,4]benzodiazepine-Gallic; QSAR, quantitative structural activity relationship; ROS, reactive oxygen species; DNA, deoxyribonucleic acid; ATR, ataxia telangiectasia mutated; ATM, ATR, ATM-Rad3-related; Chk1, checkpoint kinases 1; Bcl-xL, B-cell leukemia-xL; PARP, poly (ADP-ribose) polymerase; FTIC, fluorescein isothiocyanate; PI, propidium iodide; LMP, lysosomal membrane permeabilization.

* Corresponding author.
E-mail address: wphu@kmu.edu.tw (W.-P. Hu).

http://dx.doi.org/10.1016/j.ejmech.2015.12.039
0223-5234/

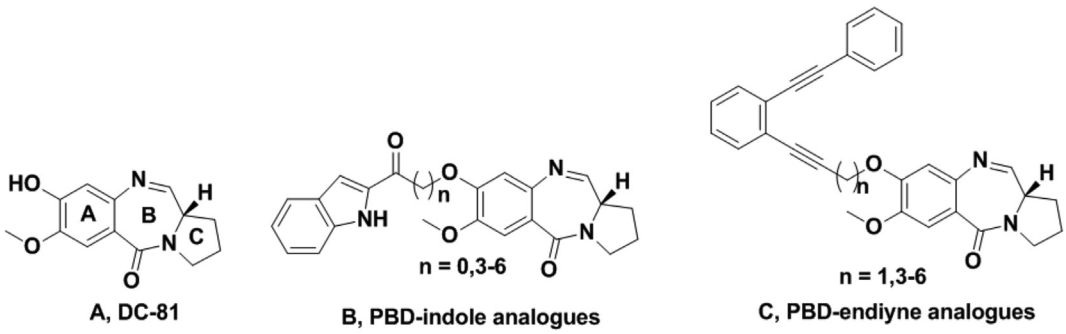

Fig. 1. Biologically active PBD derivatives.

showed that these hybrid agents have potent antitumor activity [7]. Later, this indole carboxylate-PBD hybrid with a six-carbon spacer structure (IN6CPBD) was proved to potently induce apoptosis in A375 melanoma cells through mitochondrial dysfunction and a caspase-3-mediated pathway (Fig. 1B) [8,9]. It also tends to reduce melanoma metastasis in mouse lungs, with better efficacy and superior safety than its mother compound, DC-81 [10]. By altering the spacer length, we recently elucidated the four-carbon spacer (IN4CPBD) for its anti-metastatic mechanism [11]. On the other hand, the enediyne moieties contain either DNA intercalating groups [12] or DNA minor-groove binding functions [13] and thus are considered potential DNA-damaging agents due to their ability to generate benzenoid diradicals [14]. From these previous studies, we were inspired to evaluate the molecular mechanism of PBD-enediyne conjugates for their anti-tumor activity (Fig. 1C) [15,16].

In the last few years, a number of pharmacological and biological properties have attracted attention to the development of synthetic gallic acid derivatives [17]. Gallic acid and its derivatives affect the activity of a variety of DNA and RNA [18]; they also play an important role in the prevention of inflammatory and malignant processes [19]. Gallic acid derivatives also selectivity inhibit proliferation, metastasis, and anti-apoptotic processes. These studies have revealed considerable tumor-specific cytotoxic effects in a wide variety of human and murine tumor cell lines [20]. The most important advantage of gallic acid and its derivatives is that they can selectively induce apoptosis to cancer cells without affecting the normal cells [21,22].

Several cancer cell lines have been shown to cause cell death by DNA damage-induced cell cycle arrest due to generation of reactive oxygen species (ROS) [23,24]. Human bodies are constantly exposed to exogenous or endogenous sources and antioxidants play a crucial role in preventing oxidative damage to biological molecules. Mitochondria are important and actively participate in the production of ROS. The permeabilization of the outer membrane and the subsequent pro-apoptotic protein release from the inner membrane of the mitochondria are the most crucial events in the initiation and execution of apoptosis [25].

The tumor protein p53 is activated by the deregulated expression of oncogenes, which induce replication stress and thereby cause DNA damage [26]. The p53-dependent anti-apoptotic protein Bcl-xL and the death-promoting Bax protein of the Bcl-2 family are considered requisite gateways to the mitochondrial apoptotic pathway [27]. In addition, ROS production also causes lysosome damage. Lysosomes are acidic, single-membrane bound organelles that are filled with hydrolases [28], and the cathepsin family of proteases is the best characterized [29].

Based on this previous background and our continuing research interest in the PBD conjugates, we were motivated to develop a new series of pyrrolo[2,1-c][1,4]benzodiazepine (PBD)-Gallic hybrid agents conjugated through alkyl spacers (Fig. 2), and to determine whether apoptosis was induced by p53-dependent or p53-independent mechanisms using two melanoma cell lines: A375 (wild-type p53) and RPMI7951 (mutant p53). Moreover, we were also interested in studying the in vivo efficacy of PBD-GA in the B16 murine melanoma cell tumorigenesis in skin.

2. Results and discussion

2.1. Chemistry

The synthesis of our newly designed PBD-Gallic hybrid agents was initiated from compound **1**. We have synthesized the key precursor **1** from vanillic acid according to our previous literature protocol involving 8 steps [4]. The reaction of compound **1** with various dibromoalkanes in the presence of ethyl methyl ketone and K_2CO_3 afforded the compounds **2a**–**2d** in 79–91% yields, respectively. Then, the reaction of compound **2** with commercially available 3,4,5-trimethoxy phenol **3** in the presence of K_2CO_3/CH_3CN gave compounds **4a**–**4d** in 71–87% yields. Finally, the reduction of compound **4** in the presence of lithiumborohydride ($LiBH_4$) in THF produced the desired target PBD-Gallic derivatives **5a**–**5d** in good yields, as shown in Scheme 1.

In order to compare the activity of oxygen-tethered PBD conjugates **5a**–**5d**, we synthesized the amide-tethered PBD conjugates, as shown in Scheme 2. The reaction of 3,4,5-trimethoxy benzoyl chloride **6** with various amino alcohols **7** in the presence of a base afforded the compound **8a**–**d** in 90–97% yields. The reaction of compound **8** with tosyl chloride and NaH gave the tosylated compound **9a**–**d** in 53–70% yields. The reaction of compounds **9** and **1** with K_2CO_3 in the presence of CH_3CN afforded the compound **10a**–**d** in 71–81% yields. Finally, the reduction of imine compound **10** with $LiBH_4$/THF resulted in the amide-tethered PBD-Gallic hybrid agents **11a-d,** as shown in Scheme 2. After successful synthesis of PBD-Gallic hybrids, we next evaluated their biological activity.

2.2. Biology

2.2.1. In vitro cytotoxic effects

The cytotoxic effects of the synthesized hybrid agents **5a**–**5d** and **11a**–**11d** were assessed in various human cells by MTT assay. As shown in Table 1, oxygen-tethered hybrid agents **5b** and **5c** were potently cytotoxic in the melanoma A375 cell line as compared with other agents. In addition, there was no significant cytotoxic effect in human dermal fibroblast cells. In order to confirm whether the new hybrid agent is more effective as an antiproliferative agent than DC-81 and gallic acid, we used conjugate agents **5b** and **5c** because of their greater inhibitory activity. Our data indicated that agents **5b** and **5c** exhibit greater inhibitory activity than DC-81 and gallic acid on A375 cells (Fig. 3A). Moreover, agents **5b** and **5c**

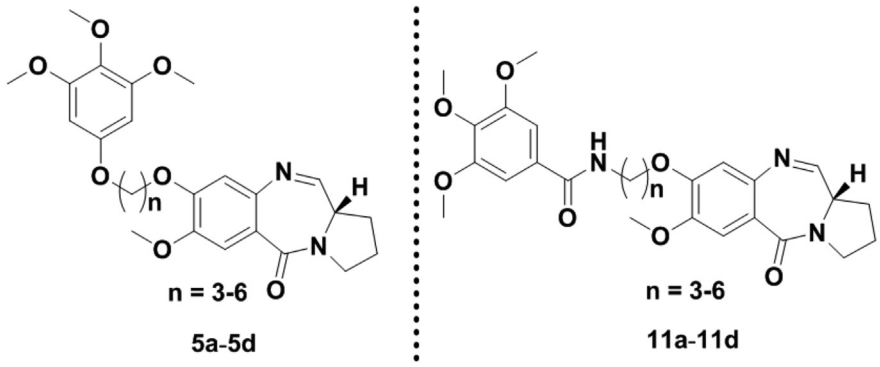

Fig. 2. PBD-Gallic hybrid agents used in this study.

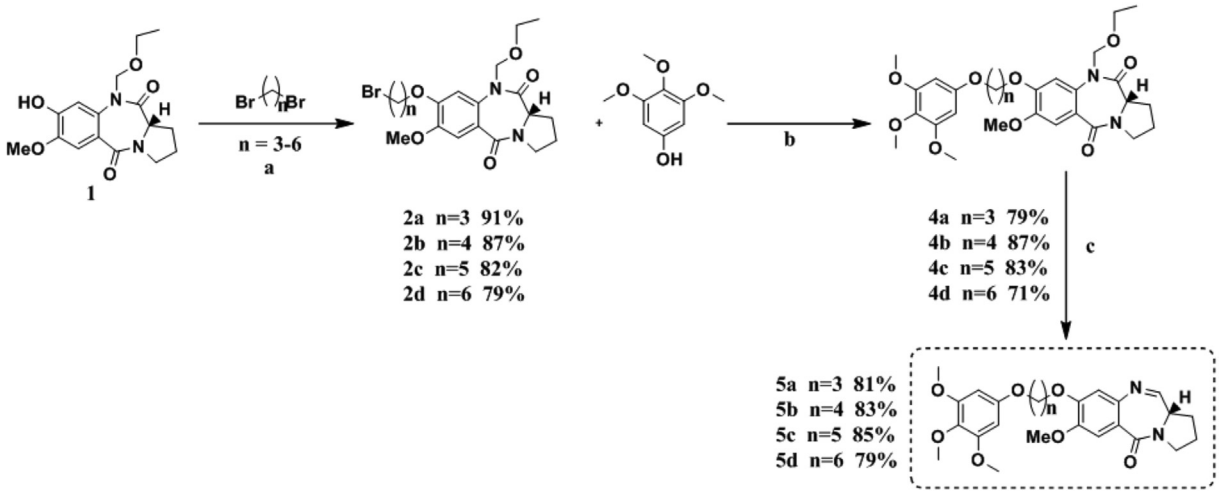

Scheme 1. Synthetic method for the PBD-Gallic hybrid agents **5a**–**5d**. Reaction condition: a) Compound **1** (1.0 equiv), K_2CO_3/EMK. b) Compound **2** (1.0 equiv), **3** (1.0 equiv), K_2CO_3/CH_3CN. c) Compound **4** (1.0 equiv), $LiBH_4$/THF.

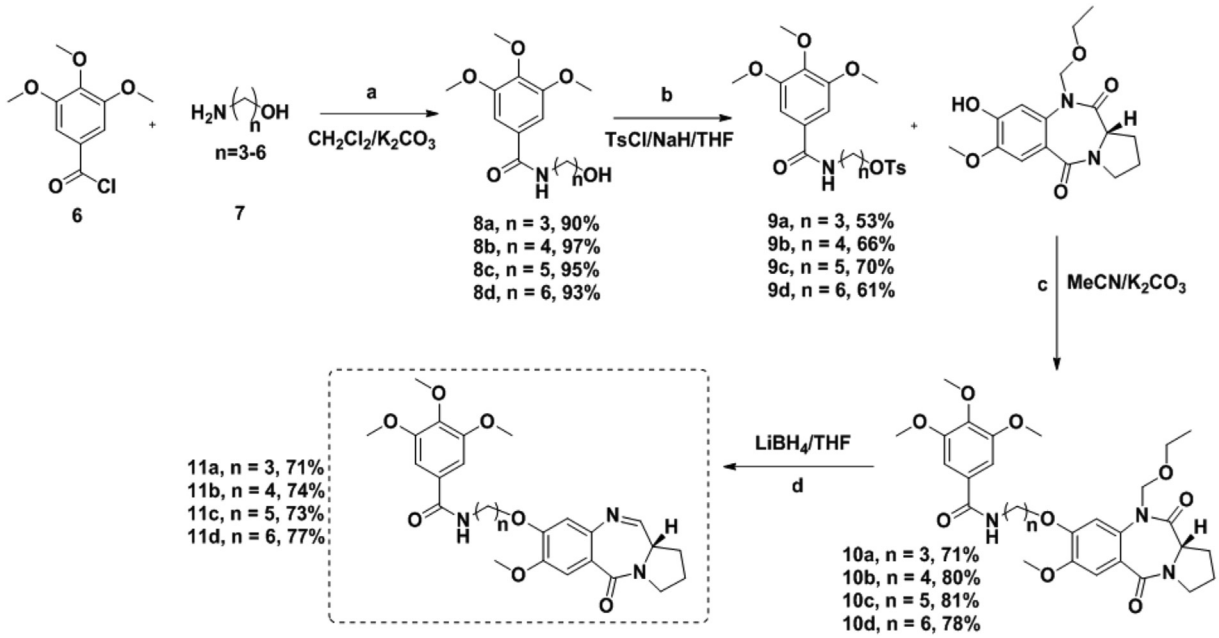

Scheme 2. Synthetic method for the PBD-Gallic hybrid agents **11a**–**11d**. Reaction condition: a) Compound **6** (1.0 equiv), K_2CO_3/CH_2Cl_2. b) Compound **8** (1.0 equiv), TsCl (1.5 equiv), NaH/THF. c) Compound **9** (1.0 equiv), 1 (1.0 equiv), K_2CO_3/CH_3CN. d) Compound **10** (1.0 equiv), $LiBH_4$/THF.

Table 1
Cytotoxic activities of compounds in different human cell lines.[a]

Compound (1 μM)	Cell lines					
	A375 (p53 wt)	RPMI7951 (p53 mutant)	MCF-7 (p53 wt)	A549	H1299 (p53 knockout)	Fibroblast (p53 wt)
5a	69.7 ± 3.4	59.5 ± 1.3	51.7 ± 4.3	88.7 ± 2.1	71.9 ± 0.7	97.3 ± 0.2
5b	37.4 ± 0.7	62.3 ± 0.7	55.3 ± 4.3	77.9 ± 2.0	73.0 ± 0.6	109.0 ± 2.0
5c	37.7 ± 0.3	64.6 ± 1.1	55.0 ± 3.6	78.0 ± 1.1	69.4 ± 2.0	110.7 ± 1.0
5d	84.8 ± 1.0	55.9 ± 0.4	79.0 ± 2.2	101.1 ± 2.4	90.2 ± 0.9	93.4 ± 0.3
11a	82.6 ± 0.5	97.7 ± 0.6	94.6 ± 3.2	96.1 ± 1.2	96.4 ± 0.4	101.1 ± 0.6
11b	79.5 ± 0.9	83.0 ± 0.7	96.3 ± 4.4	100.2 ± 3.8	95.0 ± 0.7	98.2 ± 0.3
11c	74.7 ± 0.8	111.0 ± 1.3	100.6 ± 3.5	96.8 ± 2.1	96.9 ± 1.2	98.7 ± 1.0
11d	86.5 ± 0.7	69.6 ± 0.4	95.4 ± 2.8	100.9 ± 2.3	92.4 ± 0.4	94.9 ± 0.7

[a] Cells were cultured with compounds **5a-d**, **11a-d** at a concentration of 1 μM for 24 h before growth and viability were assessed using the MTT assay.

exhibited higher inhibitory activity on A375 cells (wild-type p53) compared to RPMI7951 cells (mutant p53) at a concentration of 1 μM for 24 h in the MTT assay. Nevertheless, the inhibitory activity of PBD-Gallic agents on RPMI7951 cells as well as on A375 cells was confirmed by a colony formation assay in which the cells were treated for a longer time than in the MTT assay (Fig. 3B).

2.2.2. Molecular docking studies

The PBD core has a chiral center at the C-11 position and a DNA-reactive imine moiety at the N-10 and C-11 positions. These molecules are covalent minor groove binders and can covalently bind to a guanine base at its exocyclic 2-amino group in double-helical B-DNA (AGA-motive) [30]. These molecules are accommodated within the minor groove covering the centrally located 5–6 bp. With this a priori knowledge, the molecular docking studies were performed to study the DNA-ligand interactions of newly synthesized conjugates **5a**–**d** and **11a**–**d**. The checkpoint is if our compounds have any chance to get into the transition state before the covalent bond forms. In Supplementary Table S1, the results show that among the 50 best docking poses in terms of energy, all PBD hybrid agents showed high frequency to have the guanine base at its exocyclic 2-amino group. The distance between the C-11 of the hybrid agents and the 2-amino group of the guanine was measured and was found to be in the range of 2.7–3.7 Å. In the two illustrative docking binding modes shown in Fig. 4, the PBD hybrid agent core was positioned almost perpendicular to the guanine base in the DNA, with a C-11 carbon coordinated to the exocyclic 2-amino group of the guanine. The high transition state frequency suggests that hybrid agents **5a**–**5d** and **11a**–**11d** all have the ability to form covalent bonds with the guanine base.

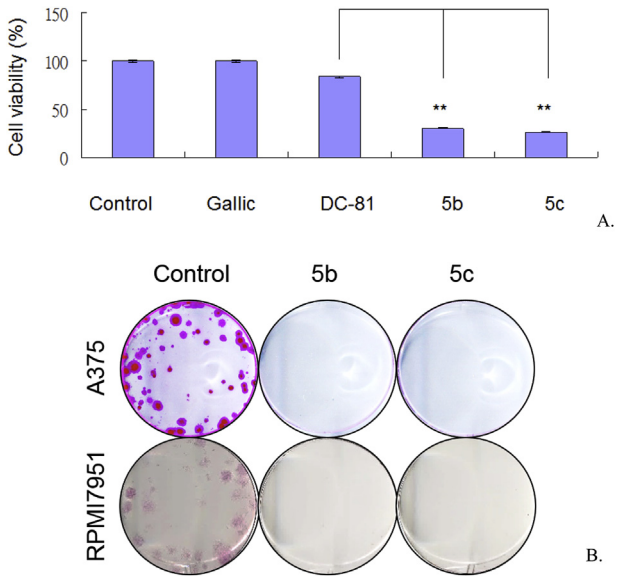

Fig. 3. Effect of PBD-Gallic on cell viability. (A) Cell viability of 0.5 μM compounds tested against A375 cells for 24 h (same experimental conditions as in Table 1). (B) Cells were plated into 6-well plates at a density of 100 cells per well. On the second day, cells were treated with PBD-Gallic. Every 3 days, the medium was replaced with fresh medium containing the agent at 0.5 μM concentration. After a 10 day treatment, the medium was removed, and cell colonies were stained with SRB dyes, and pictures were taken using a digital camera. **P < 0.01 *vs* control group. Similar results were obtained in three independent experiments.

2.2.3. Covalent interaction

We proposed that the mechanism of action of the hybrid agents is associated with their ability to form an adduct in the minor groove, thus interfering with DNA processing [32]. After insertion in the minor groove, an aminal bond is formed through nucleophilic attack of the exocyclic 2-amino group of the guanine at the electrophilic C-11 position of the PBD, as shown in the Fig. 5.

2.2.4. PBD-gallic hybrids induced ROS generation and DNA lesion

Because excessive ROS production has been identified to cause cell death in several cancers, we measured the production of intracellular H_2O_2 using a DCFH-DA probe. After being incubated for the indicated time, the cells showed a significant level of intracellular H_2O_2 at 24 h (Fig. 6A). One of the most abundant and well-characterized DNA lesions generated by oxidative stress is 8-oxoguanine [33]. The levels of this adduct in the nuclear DNA of A375 cells after PBD-Gallic hybrid administration was determined. The immunocytochemistry analysis indicated that the expression of 8-oxoguanine increased with 0.5 μM of **5b** and **5c** treatment (Fig. 6B).

2.2.5. PBD-gallic hybrid-induced ATR/ATM activation and S phase arrest in A375 cells

A previous study reported that the control of cell death is linked to the cell cycle. Cells with a defective cell cycle are more vulnerable to some anticancer agents according to numerous preclinical studies [34]. Compounds manipulating the cell cycle may be able to arrest cell growth, inhibit differentiation, and induce apoptosis. Ataxia-telangiectasia mutated (ATM) is considered a primary regulator in response to DNA double-strand breaks [35], whereas ATR (ATM-related) has been implicated primarily in the response to ultraviolet light (UV), replication blocks, and hypoxia. Checkpoint kinase 1 (Chk1) is a direct downstream target for the ATR kinase to regulate the S-phase checkpoint. A major and crucial target for Chk1 in cell cycle checkpoints is the dual-specificity phosphatase Cdc25, which dephosphorylates and activates Cdks [36,37]. In the immunocytochemistry analysis, the activation of ATR/ATM was increased after PBD-Gallic hybrid treatment (Fig. 7A). As compared with the untreated control group, cell treatment with **5b** and **5c** resulted in an increase in Chk1 phosphorylation, whereas the level

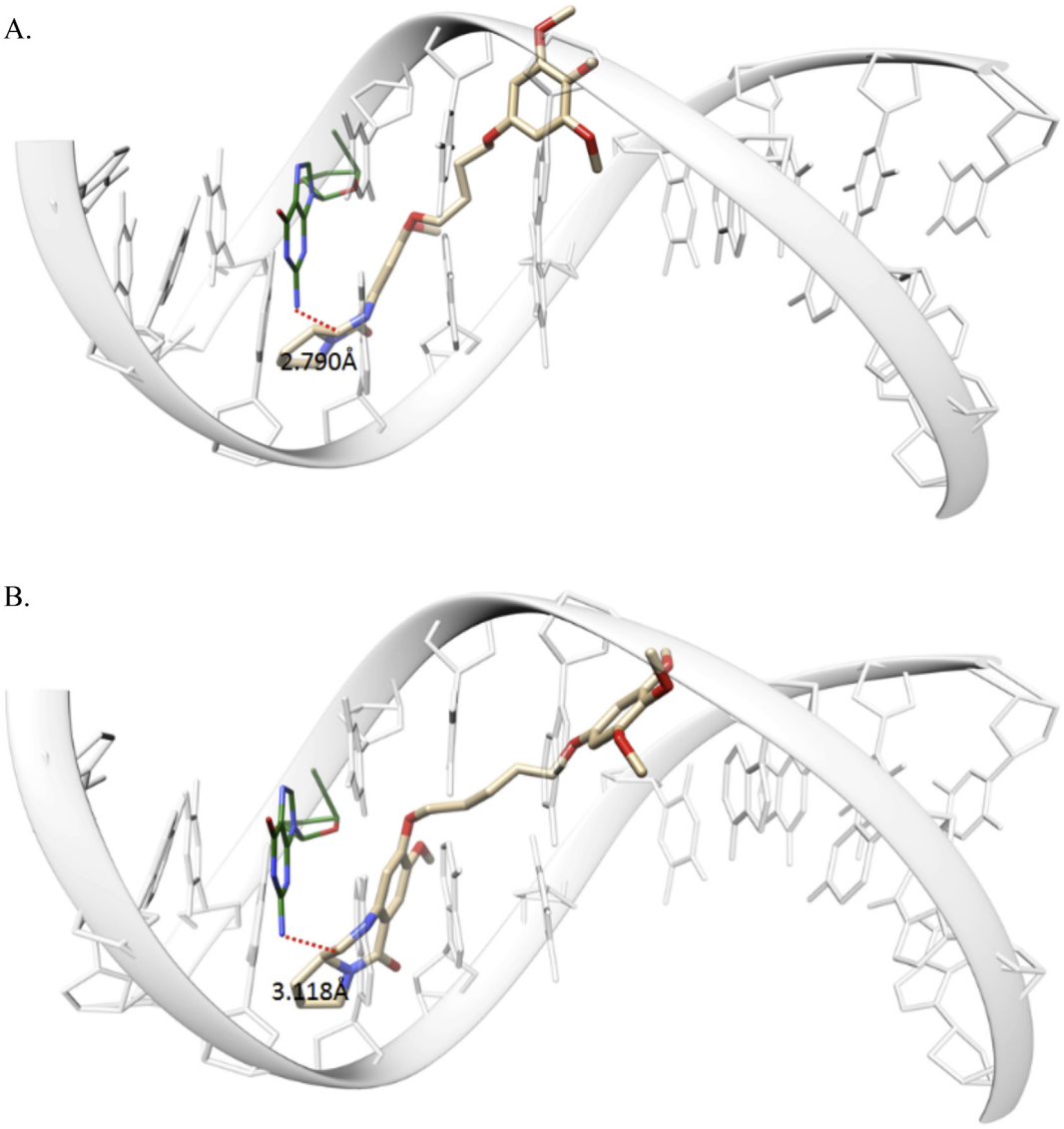

Fig. 4. Two docking binding modes of hybrid agents interaction with DNA. Hybrid agents (A) **5b** and (B) **5c** interaction with guanine base in DNA**. T**he white portion is DNA (DNA structure is from PDB ID: 2KY7 [31]), the green part is guanine of DNA and the brown part is hybrid agents **5b** or **5c**. (For interpretation of the references to color in this figure caption, the reader is referred to the web version of this article.)

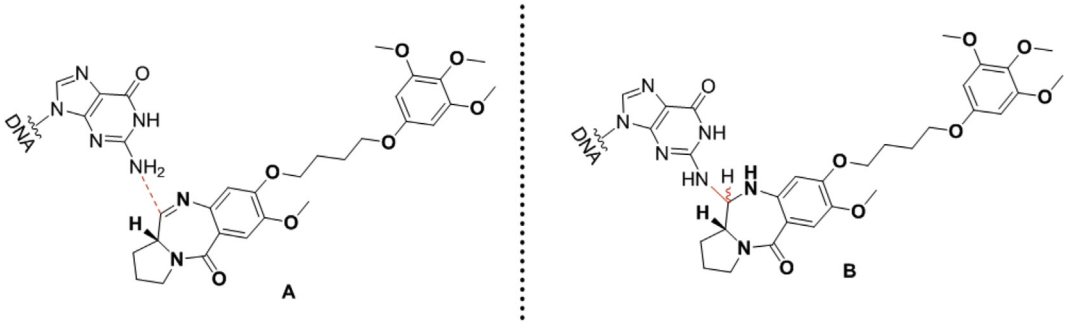

Fig. 5. Proposed mechanism (A) the view of PBD hybrid small molecule **5b** with deoxyguanosine closes to form a covalent bond. (B) The PBD hybrid agent **5b** deoxyguanosine adduct in DNA, showing formation of an aminal bond between the C-11 position of the PBD hybrid and exocyclic 2-amino group of guanine base.

of Cdc25c was reduced (Fig. 7B). Moreover, the DNA content of A375 cell nuclei was measured by flow cytometric analysis. As shown in Fig. 7C, treatment with 0.5 μM PBD-Gallic for 24 h significantly increased cell percentage at the S phase and, concomitantly, decreased cell populations at G1 and G2/M phases. The preceding results demonstrated that PBD-Gallic induces ROS generation, DNA damage, ATR/ATM and checkpoint-related signals Chk1 activation, which led to increased numbers of cells in the S

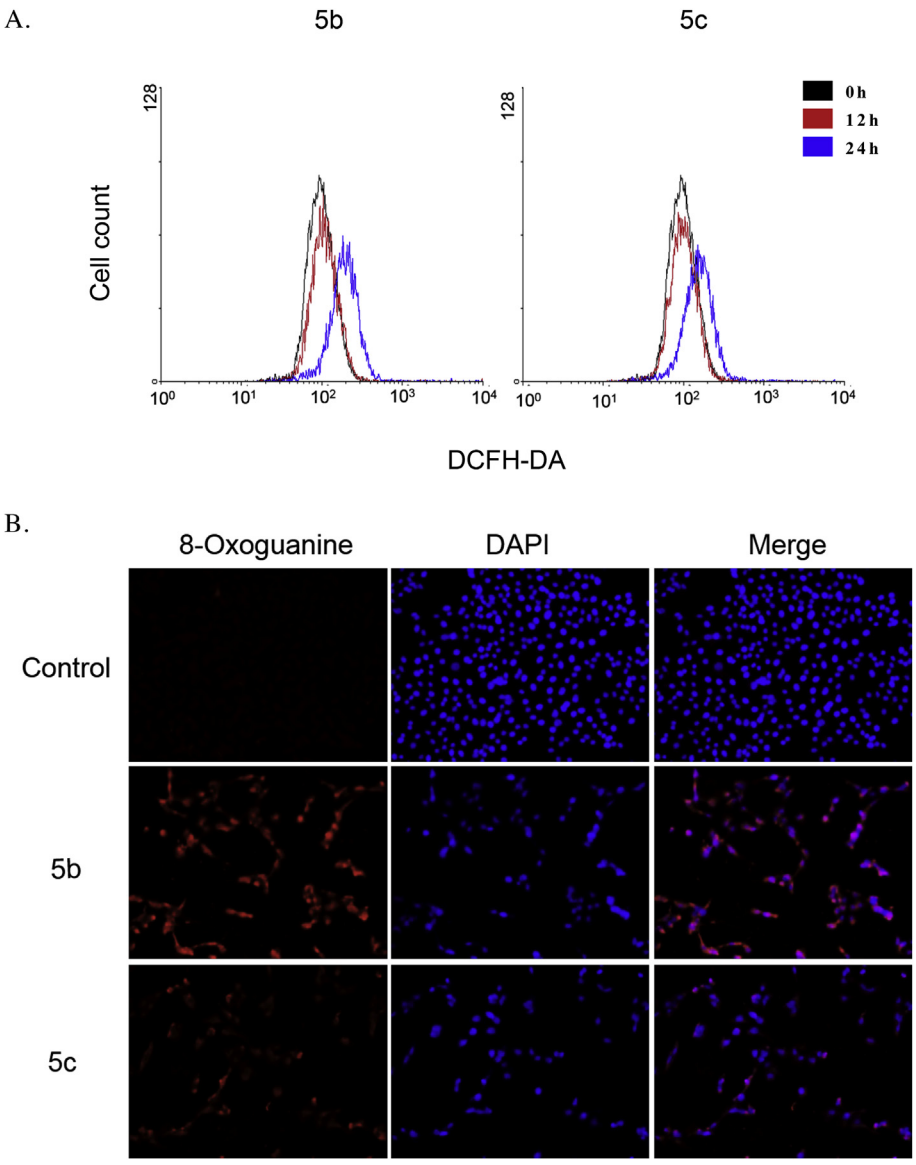

Fig. 6. PBD-Gallic induced ROS generation and DNA lesion. (A) A375 cells were treated with 0.5 μM PBD-Gallic for 0, 12, and 24 h and stained with DCFH-DA. (B) Visualization of 8-oxoguanine in the nuclear DNA of A375 cells. Cells probed with mouse anti-8-oxoguanine monoclonal antibody followed by rhodamine-labeled secondary antibody (IF, red) and counterstained with DAPI (nuclei, blue). Similar results were obtained in three independent experiments. (For interpretation of the references to color in this figure caption, the reader is referred to the web version of this article.)

phase of the cell cycle.

2.2.6. PBD-gallic hybrids induced p53-dependent mitochondrial apoptosis in A375 cells

The p53 gene is considered a tumor-suppressor gene [38], which might be a crucial regulator of cell cycle checkpoints, DNA repair and apoptosis [39]. The p53 gene is also one of the downstream targets of ATM used as a marker of DNA double-strand breaks. The p53-dependent anti-apoptotic protein Bcl-xL and the death-promoting proteins Bax of the Bcl-2 family are considered as requisite gateways to the mitochondrial apoptotic pathway [26]. Caspase-3 has been shown to be one of the most important cell executioners for apoptosis [40,41]. Poly (ADP-ribose) polymerase (PARP) has been identified as a substrate for caspase-3. The expression of apoptosis-related proteins was determined by Western blotting assay. Our results showed that apoptotic cell death triggered by **5b** and **5c** was associated with increased levels of p53, decreased levels of Bcl-xL, and cleaved both caspase-3 and PARP to identify apoptotic cells (Fig. 8A). The apoptosis-associated mRNA expressions (p53, bax, bcl-xl) of **5b**–**5c** on A375 cells are a time-dependent manner by real-time quantitative PCR (Fig. 8B). Mitochondrial membrane potential ($\Delta\Psi_{mt}$) is a vital factor for determining cellular status. The decline in $\Delta\Psi_{mt}$ is an early event in the process of cell death [42]. Therefore, we investigated whether $\Delta\Psi_{mt}$ disruption was involved in PBD-Gallic-induced apoptosis. We treated A375 cells with 0.5 μM PBD-Gallic for 0, 12, and 24 h, and then analyzed them using flow cytometry after $DiOC_6$ dye labeling. Cells treated with PBD-Gallic exhibited a significant decline in $\Delta\Psi_{mt}$ after 12 h treatment (Fig. 8C). Another assessment of mitochondrial function was to determine the translocation of cytochrome *c* from the mitochondrial intermembrane space to the cytosol [43,44]. Immunofluorescent staining showed that treating cells with 0.5 μM PBD-Gallic significantly increases the release of cytochrome *c* from mitochondria to cytosol (Fig. 8D).

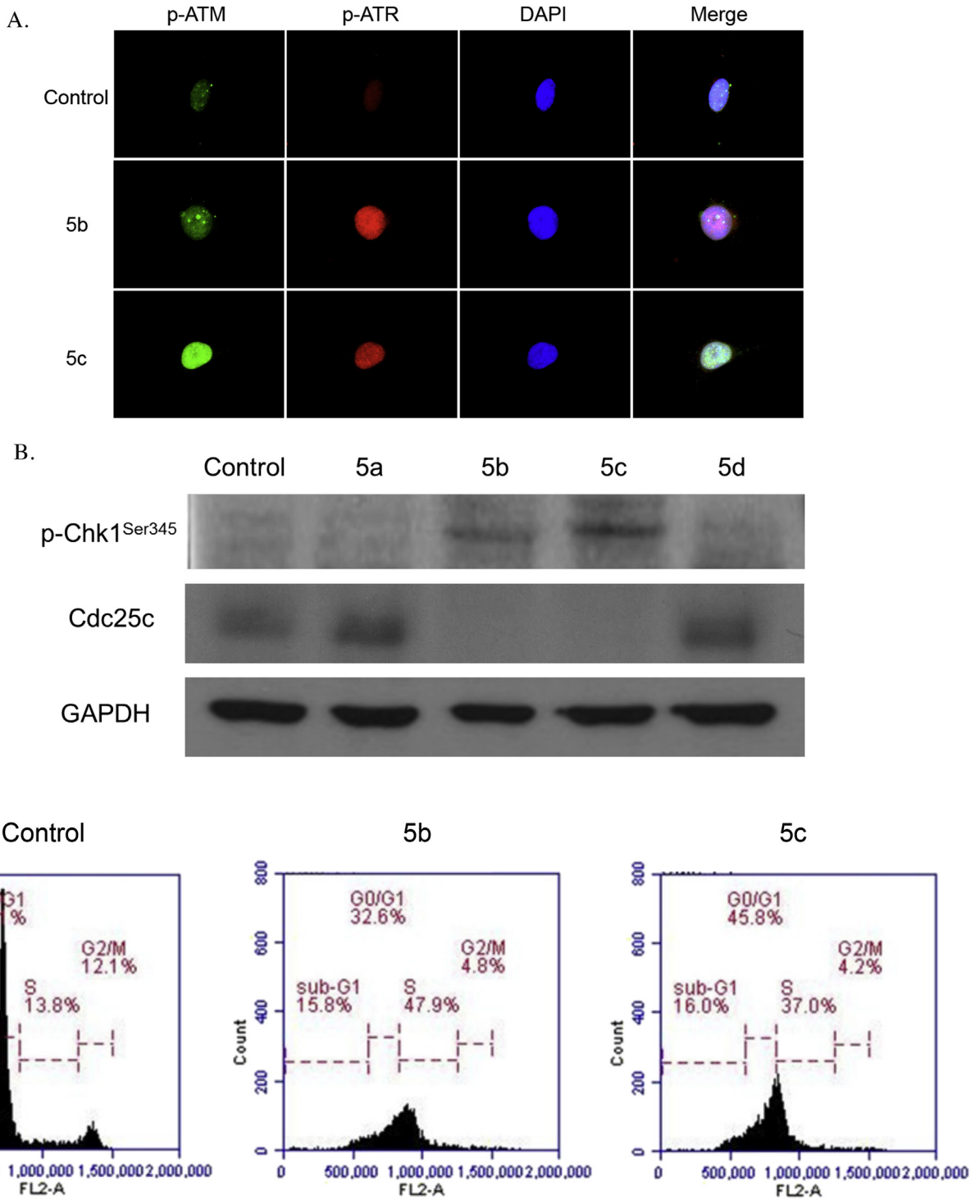

Fig. 7. Effect of PBD-Gallic on induction of DNA-damage-sensing kinases and cell cycle distribution in A375 cells. (A) Immunofluorescence staining with p-ATM (green), p-ATR (red), and DAPI (blue) in A375 cells after 0.5 μM PBD-GAs for 24 h. (B) Western blots showed the effect of PBD-Gas on the protein expression of cell cycle checkpoints in A375 cells. For the internal control, the same amounts of protein extract were also probed with antibody against GAPDH. (C) Flow cytometric analyses of cell cycle distribution of A375 cells after exposure to 0.5 μM PBD-Gallic for 24 h $^{*}p < 0.05$, $^{**}p < 0.01$ as compared with the control. Similar results were obtained in three independent experiments. (For interpretation of the references to color in this figure caption, the reader is referred to the web version of this article.)

2.2.7. PBD-gallic hybrid induced p53-independent mitochondrial apoptosis in RPMI7951 cells via LMP

Lysosomal membrane permeabilization (LMP) occurs in response to a large variety of cell death stimuli causing release of cathepsins from the lysosomal lumen into the cytosol where they participate in apoptosis signaling. Previous studies have reported that factors in LMP include DNA damage, ROS, and p53 [45,46]. To determine whether PBD-Gallic induced RPMI7951 apoptosis, which might require active p53 participation, we measured the lysosomal H^{+} concentration using the lysotracker. As shown in Fig. 9A, the wild-type p53 of A375 cells had no effect on LMP after PBD-Gallic treatment. However, a silencing of p53 decreased

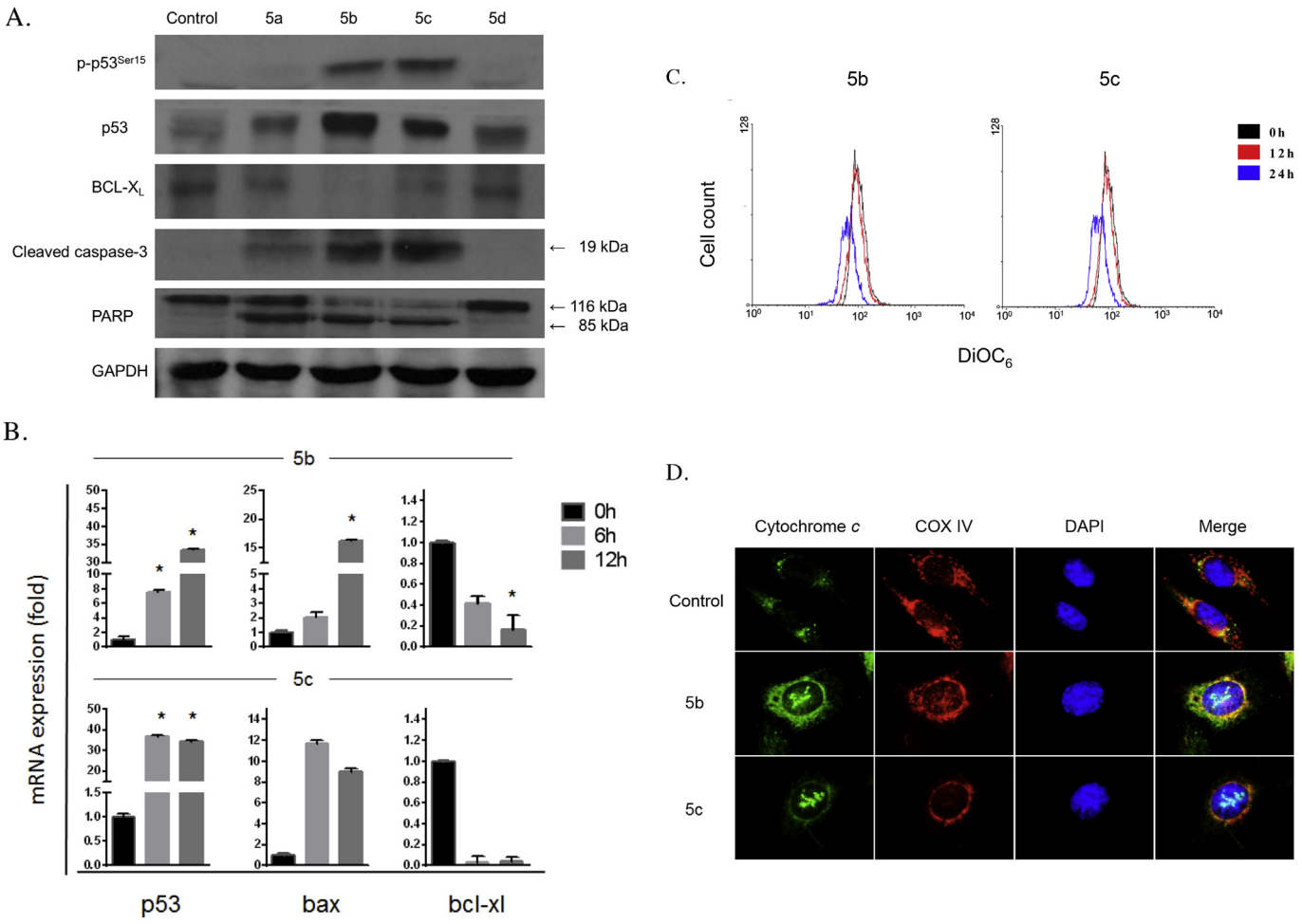

Fig. 8. Effect of PBD-Gallic on mitochondrial function and apoptosis in A375 cells. (A) After exposure to 0.5 μM PBD-Gallic for 24 h, cell lysates were collected and Western blotted with specific antibodies as indicated. (B) Expression of p53, bax, and bcl-xl mRNA in different groups. The mRNA expression analyzed by quantitative real-time PCR and the expressional levels were normalized to the level of GAPDH mRNA. (C) The $\Delta\Psi_{mt}$ of A375 cells after exposure to 0.5 μM PBD-Gallic for 24 h and stained with $DiOC_6$ then analyzed by flow cytometry. (D) Immunofluorescent staining of cytochrome c (green), the distribution of COX IV (mitochondrial marker, red), and DAPI (blue) in A375 cells. $^*p < 0.05$ *vs* control group. Similar results were obtained in three independent experiments. (For interpretation of the references to color in this figure caption, the reader is referred to the web version of this article.)

lysosomal H^+ concentration in A375 cells after 48 h PBD-Gallic treatment, as well as mutant p53 of RPMI7951. These data indicate that p53 might be independent of PBD-Gallic -induced LMP in RPMI7951 cells. Because aspartic cathepsin D is involved in mitochondrial, caspase-dependent apoptosis signaling [47,48], the extent of lysosomal damage, cytochrome *c* release, and PARP degradation of RPMI7951 cells after PBD-Gallic administration was determined. According to the immunocytochemistry analysis, the release of cathepsin and cytochrome *c* into the cytosol was increased by the PBD-Gallic (Fig. 9B–C), and data from the Western blot experiment showed degradation of PARP when RPMI7951 cells were exposed to PBD-Gallic as compared with the control group (Fig. 9D).

*2.2.8. Antitumor activity of **5b** in tumor-bearing mice*

In order to evaluate the effect of PBD-Gallic on B16 cell lines, we examined in vitro and in vivo antitumor activity (Fig. 10). Fluorescein isothiocyanate (FITC)-conjugated annexin V was utilized to detect the externalization of phosphatidylserine that occurs at an early stage of apoptosis. Propidium iodide (PI) is used as a marker of necrosis due to cell membrane destruction [49]. As demonstrated in Fig. 10A, treatment of B16 cells with 0.5 μM **5b** for 24 h resulted in more apoptotic cells than the untreated control after annexin V and PI staining. Moreover, to address whether PBD-Gallic has a better effect, we injected mouse melanoma B16 cells into the footpad of the ICR mice. Compound **5b** at various doses was delivered to the mice. We then observed the tumor sizes sequentially. Compound **5b** induced significant tumor reduction in a concentration-dependent manner, indicating the anti-cancer activity of PBD-Gallic (Fig. 10B). Furthermore, all doses of **5b** were well tolerated, as indicated by animal body weight (Fig. 10C).

3. Conclusions

In this study, we performed a series of experiments using two isogenic melanoma cell lines, A375 and RPMI7951, differing in their p53 status and potential differences in PBD-Gallic-induced cytotoxicity. The QSAR studies showed that the hybrid agents **5a**–**5d**, **11a**–**11d** are able to form a covalent bond with the minor groove of DNA. Moreover, the PBD-Gallic was able to induce DNA damage, increase cells in the S phase, activate p53, and increase mitochondrial, caspase-dependent apoptotic cell death by generating ROS in A375 cells. On the other hand, PBD-Gallic induced lysosome- and mitochondria-dependent cell apoptosis in RPMI7951 with mutant p53, as shown in Fig. 11. Furthermore,

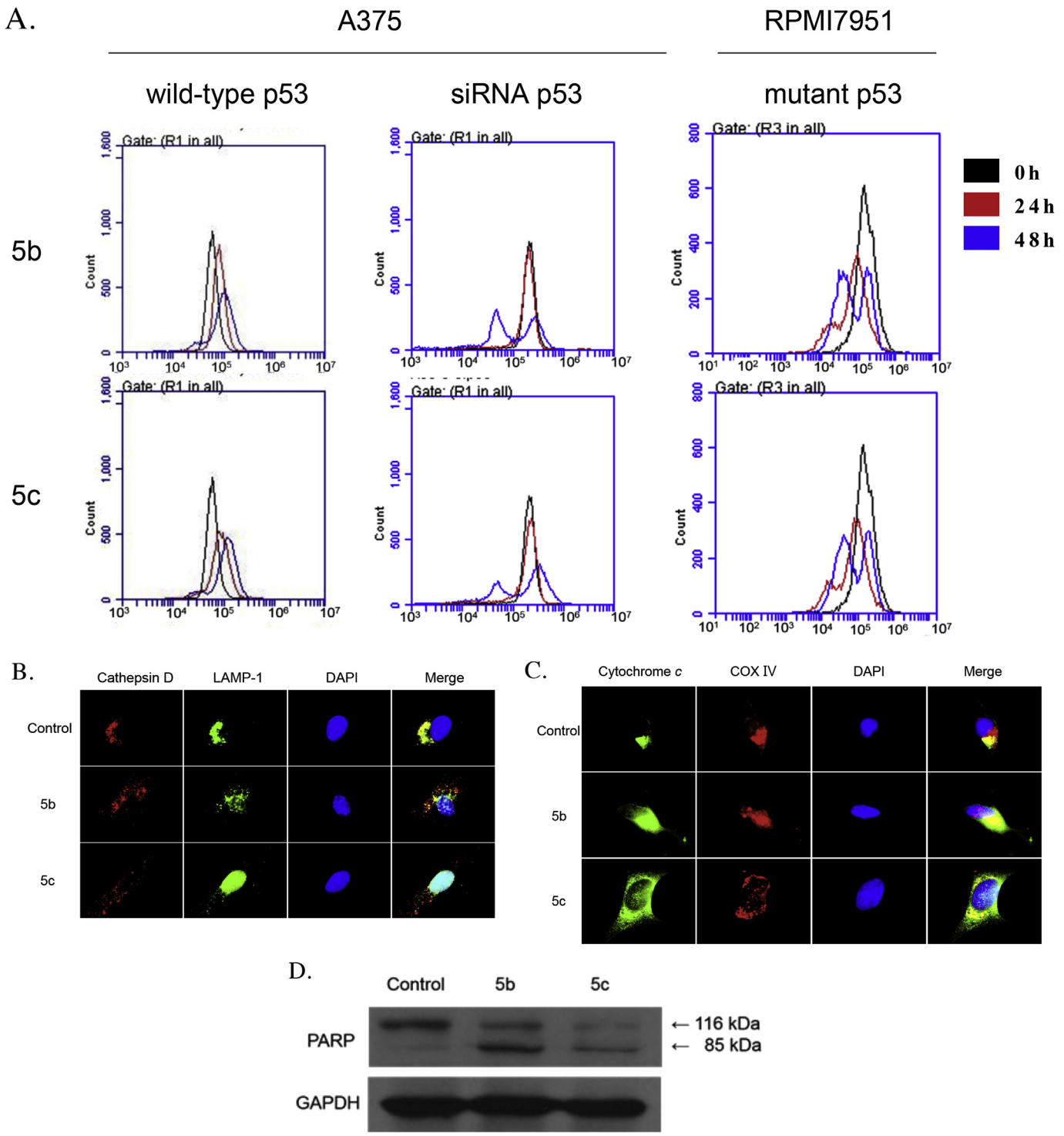

Fig. 9. PBD-Gallic result in mitochondrial apoptosis by lysosomal membrane permeabilization in RPMI7951. (A) A375 and RPMI7951 cells were treated with 0.5 μM PBD-Gallic for indicated time to determine the lysosomal H^+ concentration by lysotracker. (B) & (C) Immunofluorescent staining of cathepsin D(red), LAMP-1 (lysosomal marker, green), cytochrome c (green), the distribution of COX IV (red), and DAPI (blue) in RPMI7951 cells. (D) Induction of PARP cleavage by PBD-Gallic (same experimental conditions as in Fig. 8A). Similar results were obtained in three independent experiments. (For interpretation of the references to color in this figure caption, the reader is referred to the web version of this article.)

PBD-Gallic could induce a marked increase of annexin V binding in B16 cells and could also reduce murine melanoma size in the mouse model. This study successfully demonstrated the in vitro and in vivo efficacy of PBD-Gallic in B16 melanoma cell tumorigenesis in ICR mice. Finally, we revealed a novel PBD-Gallic antitumor proliferation mechanism and we suggest that these agents may have potential chemotherapeutic activity for melanomas with wild type p53 or mutant p53.

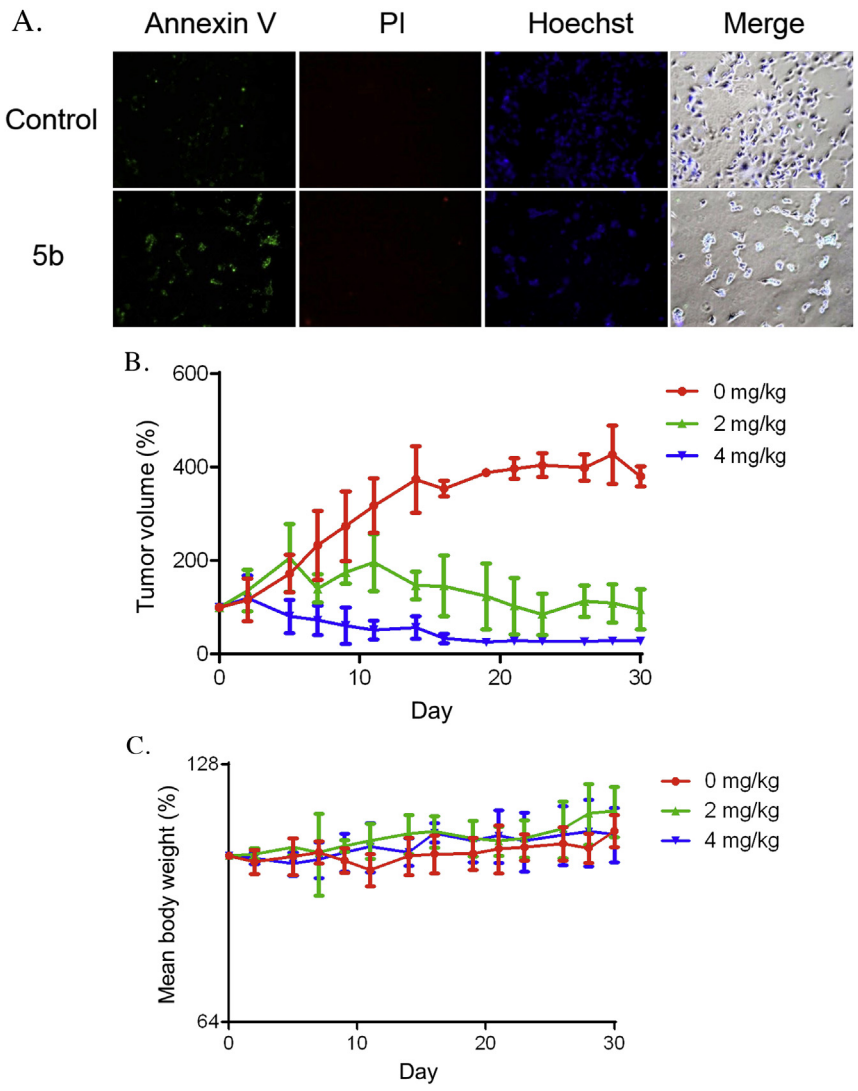

Fig. 10. Effect of compound 5b on cell apoptosis and tumor volume of B16 cells. (A) B16 cells treated with 0.5 μM 5b for 24 h and then stained with PI (red), Hoechst33258 (blue), and an annexin V-FITC conjugate (green) specifically detecting the exposure of PS residues at the cell surface. (B) Tumor was established by injection of 5×10^6 cells/mL of B16 into each sole of feet of the female ICR mice. (C) Animal body weight plotted as a percentage of that on day 0. (For interpretation of the references to color in this figure caption, the reader is referred to the web version of this article.)

4. Experimental section

4.1. Chemistry

4.1.1. Materials and methods

^{1}H NMR and ^{13}C NMR spectra were recorded on a OXFORD 200 spectrometer or a Varian Mercury Plus 400 spectrometer. The chemical shift (δ) values are reported in ppm, and the coupling constants (J) are given in Hz. The spectra were recorded using $CDCl_3$ or DMSO-d6 as a solvent. ^{1}H NMR chemical shifts are referenced to TMS (0 ppm) or $CDCl_3$ (7.26 ppm). ^{13}C NMR was referenced to $CDCl_3$ (77.0 ppm). The abbreviations used are as follows: s, singlet; bs, broad singlet; d, doublet; dd, double doublet; t, triplet; m, multiplet Mass spectra and high resolution mass spectra (HRMS) were measured using the ESI. All products reported showed ^{1}H NMR spectra in agreement with the assigned structures. The purity of the tested compounds were analyzed by reverse-phase HPLC (Waters Spherisorb R S10 0DS2; 20 × 250 mm semi-prep column) using an Waters 600 HPLC Pump system equipped with a Waters 2487 dual λ absorbance detector. The mobile phase used was CH_3CN and H_2O. All tested compounds yielded data consistent with a purity of at least 98%. Reaction progress and product mixtures were routinely monitored by TLC using Merck TLC aluminum sheets (silica gel 60 F254), and also visualized with aqueous KMnO4. Column chromatography was carried out with 230–400 mesh silica gel 60 (Merck). All chemicals and reagents were purchased from commercial suppliers (Sigma Aldrich, Alfa Aesar and Merck) and were used without further purification.

4.1.2. Procedure for the synthesis of compound ***2a–2d***

To a solution of compound **1** (0.63 mmol) in ethyl methyl ketone (EMK) as solvent (10 mL) in a 100 mL round bottom flask was cooled to 0 °C. Then the reaction mixture was charged with potassium carbonate (1.89 mmol) and continued stirring for another 30 min at the same temperature. Finally, the corresponding dibromo compound was added and allowed to reach room temperature gradually and stirred for 6hr. The completion of the reaction was monitored by TLC chromatogram. The reaction was quenched with ice water and extracted with dichloromethane and dried over Na_2SO_4. The removal of solvent under reduced pressure

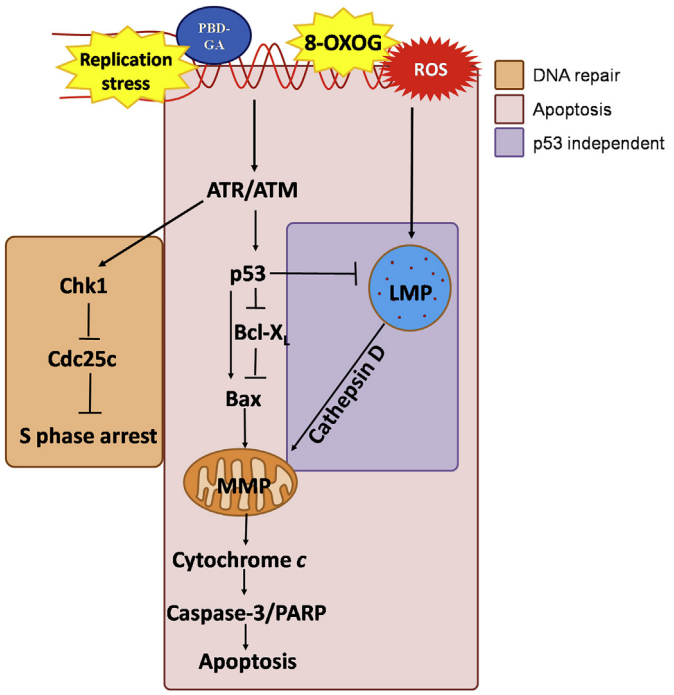

Fig. 11. A proposed mechanism for PBD-Gallic -induced melanoma apoptosis with p53-dependent A375 cells or p53-independent RPMI7951 cells.

gave the crude compounds **2a**–**2d**. The crude compounds were further purified by column chromatography using dichloromethane/methanol ratio 150:1 to afford the pure compounds in 79–81% yields respectively.

*4.1.3. Procedure for the synthesis of compound **4a**–**4d***

To as solution of compound **2** (0.45 mmol) in acetonitrile (10 mL) in a 100 mL round bottom flask was cooled to 0 °C. To this cooled solution potassium carbonate (1.35 mmol) was charged and continued the stirring for another 30 min at the same temperature. Then the 3,4,5- Trimethoxyphenol (0.68 mmol) was added and stirred at 80 °C for 24 h. The completion of the reaction was monitored with the help of TLC chromatogram. The reaction was quenched with ice water and extracted with dichloromethane and dried over Na_2SO_4. The removal of solvent under reduced pressure gave the crude compounds **4a**–**4d**. The crude compounds were further purified by column chromatography using dichloromethane/Methanol ratio 70:1 to afford the pre compounds in 71–87% yields respectively.

*4.1.4. Procedure for the synthesis of compound **5a**–**5d***

To a solution of compound **4** (0.37 mmol) in THF (10 mL) in a 100 mL round bottom flask was cooled to −15 °C for 30 min. To this cooled solution was added $LiBH_4$ (0.74 mmol) and continued the stirring at same temperature for 48 h. The completion of the reaction was monitored by TLC. The reaction was quenched with ice water and extracted with dichloromethane and dried over Na_2SO_4. The pure compounds **5a**–**5d** were obtained by using preparative HPLC and further by freeze drying in 79–85% yields respectively.

*4.1.5. Procedure for the synthesis of compound **8a**–**8d***

To a solution of compound **6** (4.3 mmol) in CH_2Cl_2 in 250 mL round bottom flask was cooled in an ice bath followed by the addition of K_2CO_3 (12.9 mmol) and stirred for about 30 min. Then the solution of corresponding amino butanol (6.45 mmol) was added slowly and stirred at room temperature for 24 h. The completion of the reaction was monitored by TLC chromatogram. The reaction was quenched with ice water and extracted with dichloromethane. The organic layer was given a brine wash and dried over Na_2SO_4 and concentrated under reduced pressure to afford the crude compound. The product was purified by column chromatography using methylene chloride: methanol = 70: 1–50: 1 to obtain the pure compounds **8a**–**8d** in 90–97% yields respectively.

*4.1.6. Procedure for the synthesis of compound **9a**–**9d***

To a solution of compound **8** (0.71 mmol) in THF (10 mL) CH_2Cl_2 in 250 mL round bottom flask was cooled to −15 °C. To this cooled solution sodium hydride (2.13 mmol) was added and stirred for 30 min. Finally, tosyl chloride (0.85 mmol) was added to the reaction mixture and stirred under −15 °C for 1 h. The completion of the reaction was monitored by TLC chromatogram. The reaction was quenched with ice water and extracted with dichloromethane. The dichloromethane layer was give brine and water wash. The resulting solution was dried over $NaSO_4$ and concentrated under reduced pressure to give the crude compound. This was further purified by column chromatography using ethyl acetate/hexane to afford the pure compounds **9a**–**9d** in 53–70%.

*4.1.7. Procedure for the synthesis of compound **10a**–**10d***

To as solution of compound **1** (0.63 mmol) in acetonitrile (10 mL) in a 100 mL round bottom flask was cooled to 0 °C. To this cooled solution potassium carbonate (1.89 mmol) was charged and continued the stirring for another 30 min at the same temperature. Then the corresponding compound **9** (0.76 mmol) was added and stirred at rt for 24 h. The completion of the reaction was monitored with the help of TLC chromatogram. The reaction was quenched with ice water and extracted with dichloromethane and dried over Na_2SO_4. The removal of solvent under reduced pressure gave the crude compounds **10a**–**10d**. The crude compounds were further purified by column chromatography using dichloromethane/Methanol ratio 100:1 to afford the pure compounds in 71–81% yields respectively.

*4.1.8. Procedure for the synthesis of compound **11a**–**11d***

To a solution of compound **10** (0.34 mmol) in THF (10 mL) in a 100 mL round bottom flask was cooled to −15 °C for 30 min. To this cooled solution was added $LiBH_4$ (0.70 mmol) and continued the stirring at same temperature for 48 h. The completion of the reaction was monitored by TLC. The reaction was quenched with ice water and extracted with dichloromethane and dried over Na_2SO_4. The pure compounds **11a**–**11d** were obtained by using preparative HPLC and further by freeze drying in 71–77%.

4.1.9. Spectral characterization for compounds 2, 4, 5, 8, 9, 10 and 11

*4.1.9.1. (S)-8-(3-bromopropoxy)-7-methoxy-1,2,3,11a-tetrahydro-5H-benzo[e]pyrrolo[1,2-a][1,4]diazepin-5-one (**2a**).* Yellow color oil; Yield: 91%; ^{1}H NMR ($CDCl_3$, 400 MHz) δ 7.36 (s, 1H), 7.29 (s, 1H), 5.58 (d, J = 10 Hz, 1H), 4.66 (d, J = 10 Hz, 1H), 4.24–4.13 (m, 3H), 3.92 (s, 3H), 3.80–3.73 (m, 2H), 3.70–3.64 (m, 2H), 3.61–3.53 (m, 2H), 2.74–2.70 (m, 1H), 2.44–2.37 (m, 2H), 2.13–1.98 (m, 3H), 1.26 (t, J = 7.2 Hz, 3H); ^{13}C NMR ($CDCl_3$, 100 MHz) δ 170.1, 164.9, 150.7, 147.2, 133.7, 122.3, 111.3, 106.9, 78.0, 66.4, 64.7, 57.4, 55.9, 46.5, 31.8, 29.6, 26.4, 23.6, 15.2; HRMS (ESI, m/z) $C_{19}H_{25}BrN_2O_5$ calcd 441.1025 found 441.1028.

*4.1.9.2. (S)-8-(4-bromobutoxy)-7-methoxy-1,2,3,11a-tetrahydro-5H-benzo[e]pyrrolo[1,2-a][1,4]diazepin-5-one (**2b**).* Yellow color oil; Yield: 87%; ^{1}H NMR ($CDCl_3$, 400 MHz) δ 7.36 (s, 1H), 7.25 (s, 1H),

5.57 (d, J = 10.0 Hz, 1H), 4.65 (d, J = 10 Hz, 1H), 4.14–4.05 (m, 3H), 3.92 (s, 3H), 3.80–3.73 (m, 2H), 3.70–3.64 (m, 2H), 3.62–3.51 (m, 2H), 2.73–2.70 (m, 1H), 2.13–1.98 (m, 7H), 1.27 (t, J = 7.2 Hz, 3H); ^{13}C NMR ($CDCl_3$, 100 MHz) δ 170.1, 164.9, 150.8, 147.0, 133.7, 121.9, 111.2, 106.4, 78.0, 67.8, 64.6, 57.3, 55.9, 46.5, 33.1, 29.1, 27.4, 26.3, 23.5, 15.2; HRMS (ESI, m/z) $C_{20}H_{27}BrN_2O_5$ calcd 455.1181 found 455.1178.

*4.1.9.3. (S)-8-((5-bromopentyl)oxy)-7-methoxy-1,2,3,11a-tetrahydro-5H-benzo[e]pyrrolo[1,2-a][1,4]diazepin-5-one (**2c**).* Yellow color oil; Yield: 82%; ^{1}H NMR ($CDCl_3$, 400 MHz) δ 7.36 (s, 1H), 7.25 (s, 1H), 5.58 (d, J = 10.0 Hz, 1H), 4.64 (d, J = 10 Hz, 1H), 4.14–4.01 (m, 3H), 3.92 (s, 3H), 3.80–3.73 (m, 2H), 3.70–3.65 (m, 2H), 3.45 (t, J = 6.8 Hz, 2H), 2.74–2.70 (m, 1H), 2.13–1.87 (m, 7H), 1.69–1.61 (m, 2H), 1.27 (t, J = 7.2 Hz, 3H); ^{13}C NMR ($CDCl_3$, 100 MHz) δ 170.2, 165.0, 151.0, 147.1, 133.7, 121.9, 111.2, 106.4, 78.0, 68.5, 64.7, 57.4, 56.0, 46.5, 33.3, 32.2, 27.9, 26.4, 24.5, 23.6, 15.2; HRMS (ESI, m/z) $C_{21}H_{29}BrN_2O_5$ calcd 469.1338 found 469.1340.

*4.1.9.4. (S)-8-((6-bromohexyl)oxy)-7-methoxy-1,2,3,11a-tetrahydro-5H-benzo[e]pyrrolo[1,2-a][1,4]diazepin-5-one (**2d**).* Yellow color oil; Yield: 79%; ^{1}H NMR ($CDCl_3$, 400 MHz) δ 7.35 (s, 1H), 7.25 (s, 1H), 5.58 (d, J = 10.0 Hz, 1H), 4.66 (d, J = 10 Hz, 1H), 4.16–4.02 (m, 3H), 3.93 (s, 3H), 3.79–3.73 (m, 2H), 3.70–3.53 (m, 2H), 3.43 (t, J = 6.8 Hz, 2H), 2.74–2.69 (m, 1H), 2.11–1.88 (m, 7H), 1.55–1.51 (m, 4H), 1.27 (t, J = 7.2 Hz, 3H); ^{13}C NMR ($CDCl_3$, 100 MHz) ä 170.0, 164.8, 150.9, 146.9, 133.6, 121.6, 111.0, 106.2, 77.9, 68.5, 64.5, 57.2, 55.8, 46.4, 33.4, 32.3, 28.3, 27.5, 26.2, 24.8, 23.4, 15.1; HRMS (ESI, m/z) $C_{22}H_{31}BrN_2O_5$ calcd 483.1494 found 483.1492.

*4.1.9.5. (S)-10-(ethoxymethyl)-7-methoxy-8-(3-(3,4,5-trimethoxyphenoxy)propoxy)-1,2,3,11a-tetrahydro-5H-benzo[e]pyrrolo[1,2-a][1,4]diazepine-5,11(10H)-dione (**4a**).* Light yellow oil; Yield: 79%; ^{1}H NMR ($CDCl_3$, 400 MHz) δ 7.36 (s, 1H), 7.29 (s, 1H), 6.17 (s, 2H), 5.56 (d, J = 10 Hz, 1H), 4.67 (d, J = 10.0 Hz, 1H), 4.29–4.23 (m, 2H), 4.17 (t, J = 6.0 Hz, 2H), 4.13–4.11 (m,1H), 3.92 (s, 3H), 3.84 (s, 6H), 3.78 (s, 3H), 3.77–3.69 (m, 2H), 3.67–3.53 (m,2H), 2.73–2.69 (m, 1H), 2.37–2.31 (m, 2H), 2.13–1.98 (m,3H), 1.26 (t, J = 7.2 Hz, 3H); ^{13}C NMR ($CDCl_3$, 100 MHz) δ 170.1, 164.9, 155.2, 153.5, 150.9, 147.1, 133.7, 132.1, 122.1, 111.2, 106.6, 92.1, 77.9, 65.3, 64.6, 64.4, 60.8, 57.4, 55.9, 55.8, 46.5, 28.9, 26.3, 23.5, 15.1; HRMS (ESI, m/z) $C_{28}H_{36}N_2O_9Na$ calcd 567.2318 found 567.2317.

*4.1.9.6. (S)-10-(ethoxymethyl)-7-methoxy-8-(4-(3,4,5-trimethoxyphenoxy)butoxy)-1,2,3,11a-tetrahydro-5H-benzo[e]pyrrolo[1,2-a][1,4]diazepine-5,11(10H)-dione (**4b**).* Light yellow oil; Yield: 87%; ^{1}H NMR ($CDCl_3$, 400 MHz) δ 7.36 (s, 1H), 7.28 (s, 1H), 6.16 (s, 2H), 5.58 (d, J = 10.0 Hz, 1H), 4.68 (d, J = 10 Hz, 1H), 4.15–4.12 (m, 3H), 4.03 (t, J = 6.0 Hz, 2H), 3.89 (s, 3H), 3.84 (s, 6H), 3.81 (s, 3H), 3.74–3.66 (m, 2H), 3.64–3.43 (m, 2H), 2.74–2.68 (m, 1H), 2.18–1.96 (m, 7H), 1.26 (t, J = 7.2 Hz, 3H); ^{13}C NMR ($CDCl_3$, 100 MHz) δ 170.4, 165.6, 155.8, 153.8, 151.5, 147.4, 134.1, 132.3, 121.9, 111.5, 106.7, 92.4, 78.3, 68.8, 67.8, 65.0, 61.1, 57.8, 56.2, 56.0, 46.9, 26.7, 26.2, 25.8, 23.9, 15.5; HRMS (ESI, m/z) $C_{29}H_{38}N_2O_9Na$ calcd 581.2457 found 581.2478.

*4.1.9.7. (S)-10-(ethoxymethyl)-7-methoxy-8-((5-(3,4,5-trimethoxyphenoxy)pentyl)oxy)-1,2,3,11a-tetrahydro-5H-benzo[e]pyrrolo[1,2-a][1,4]diazepine-5,11(10H)-dione (**4c**).* Light yellow oil; Yield: 83%; ^{1}H NMR ($CDCl_3$, 400 MHz) δ 7.36 (s, 1H), 7.26 (s, 1H), 6.15 (s, 2H), 5.58 (d, J = 10.0 Hz, 1H), 4.65 (d, J = 10 Hz, 1H), 4.14–3.98 (m, 3H), 3.97 (t, J = 6.0 Hz, 2H), 3.92 (s, 3H), 3.84 (s, 6H), 3.80 (s, 3H), 3.77–3.64 (m, 2H), 3.63–3.53 (m, 2H), 2.74–2.69, (m,1H), 2.11–1.84 (m, 7H), 1.72–1.66 (m, 2H), 1.27 (t, J = 7.2 Hz, 3H); ^{13}C NMR ($CDCl_3$, 100 MHz) δ 170.2, 165.0, 155.5, 153.5, 151.1, 147.1, 133.8, 132.1, 121.9, 111.2, 106.4, 92.1, 78.1, 68.7, 67.8, 64.7, 60.9, 57.4, 56.0, 55.9, 46.6, 28.9, 28.5, 26.4, 23.6, 22.5, 15.2; HRMS (ESI, m/z) $C_{30}H_{40}N_2O_9Na$ calcd 595.2631 found 595.2634.

*4.1.9.8. (S)-10-(ethoxymethyl)-7-methoxy-8-((6-(3,4,5-trimethoxyphenoxy)hexyl)oxy)-1,2,3,11a-tetrahydro-5H-benzo[e]pyrrolo[1,2-a][1,4]diazepine-5,11(10H)-dione (**4d**).* Light yellow oil; Yield: 71%; ^{1}H NMR ($CDCl_3$, 400 MHz) δ 7.35 (s, 1H), 7.25 (s, 1H), 6.15 (s, 2H), 5.58 (d, J = 10 Hz, 1H), 4.64 (d, J = 10 Hz, 1H), 4.13–4.03 (m, 3H), 3.94 (t, J = 6 Hz, 2H), 3.92 (s, 3H), 3.84 (s, 6H), 3.78 (s,3H), 3.76–3.72 (m, 2H), 3.69–3.53 (m, 2H), 2.73–2.70 (m, 1H), 2.13–1.99 (m, 3H), 1.97–1.80 (m, 4H), 1.61–1.55 (m, 4H), 1.26 (t, J = 7.2 Hz, 3H); ^{13}C NMR ($CDCl_3$, 100 MHz) δ 170.3, 165.1, 155.6, 153.6, 151.2, 147.2, 133.9, 132.1, 121.9, 111.3, 106.5, 92.1, 78.1, 68.9, 68.0, 64.7, 60.9, 57.5, 56.0, 55.9, 46.6, 29.1, 28.8, 26.5, 25.8, 25.7, 23.7, 15.3; HRMS (ESI, m/z) $C_{31}H_{42}N_2O_9Na$ calcd 609.2788 found 609.2784.

*4.1.9.9. (S)-7-methoxy-8-(3-(3,4,5-trimethoxyphenoxy)propoxy)-1,2,3,11a-tetrahydro-5H-benzo[e]pyrrolo[1,2-a][1,4]diazepin-5-one (**5a**).* Light yellow oil; Yield: 81%; ^{1}H NMR ($CDCl_3$, 400 MHz) δ 7.67 (d, J = 4.4 Hz, 1H), 7.52 (s, 1H), 6.86 (s, 1H), 6.16 (s, 2H), 4.36–4.21 (m, 1H), 4.15 (t, J = 6 Hz, 2H), 3.94 (s, 3H), 3.83 (s, 6H), 3.78 (s, 3H), 3.72–3.54 (m, 3H), 3.48 (s, 1H), 2.37–2.30 (m, 4H), 2.10–1.98 (m, 2H); ^{13}C NMR ($CDCl_3$, 100 MHz) δ 164.6, 162.4, 155.4, 153.6, 150.6, 147.7, 140.6, 132.3, 120.3, 111.6, 110.6, 95.7, 92.3, 60.9, 56.2, 56.1, 56.0, 53.7, 46.6, 29.6, 29.3, 24.1; HRMS (ESI, m/z) $C_{25}H_{30}N_2O_7$ calcd 470.5220 found 470.5223.

*4.1.9.10. (S)-7-methoxy-8-(4-(3,4,5-trimethoxyphenoxy)butoxy)-1,2,3,11a-tetrahydro-5H-benzo[e]pyrrolo[1,2-a][1,4]diazepin-5-one (**5b**).* Light yellow oil; Yield: 83%; ^{1}H NMR ($CDCl_3$, 400 MHz) δ 7.66 (d, J = 4.4 Hz, 1H), 7.50 (s, 1H), 6.81 (s, 1H), 6.14 (s, 2H), 4.20–4.07 (m, 1H), 4.00 (t, J = 6.0 Hz, 2H), 3.92 (s, 3H), 3.84 (s, 6H), 3.77 (s, 3H), 3.74–3.54 (m, 3H), 3.47 (s, 1H), 2.34–2.28 (m, 2H), 2.10–1.93 (m, 6H); ^{13}C NMR ($CDCl_3$, 100 MHz) δ 164.6, 162.4, 155.6, 153.6, 150.7, 147.7, 140.5, 132.1, 120.2, 111.5, 110.4, 95.8, 92.1, 60.9, 56.2, 56.1, 56.0, 53.6, 46.6, 29.6, 29.3, 25.9, 24.1; HRMS (ESI, m/z) $C_{26}H_{32}N_2O_7$ calcd 484.5490 found 484.5490.

*4.1.9.11. (S)-7-methoxy-8-((5-(3,4,5-trimethoxyphenoxy)pentyl)oxy)-1,2,3,11a-tetrahydro-5H-benzo[e]pyrrolo[1,2-a][1,4]diazepin-5-one (**5c**).* Light yellow oil; Yield: 85%; ^{1}H NMR ($CDCl_3$, 400 MHz) δ 7.67 (d, J = 4.4 Hz, 1H), 7.52 (s, 1H), 6.81 (s, 1H), 6.15 (s, 2H), 4.17–4.02 (m, 1H), 3.96 (t, J = 6.0 Hz, 2H), 3.94 (s, 3H), 3.86 (s, 6H), 3.79 (s, 3H), 3.74–3.55 (m, 3H), 3.48 (s, 1H), 2.36–2.30 (m, 2H), 2.10–1.83 (m, 6H), 1.70–1.63 (m, 2H); ^{13}C NMR ($CDCl_3$, 100 MHz) δ 164.6, 162.4, 155.7, 153.7, 150.8, 147.8, 140.6, 132.2, 120.2, 111.6, 110.5, 92.2, 68.8, 67.9, 61.0, 56.2, 56.1, 53.7, 46.6, 29.6, 29.0, 28.7, 24.2, 22.6; HRMS (ESI, m/z) $C_{27}H_{34}N_2O_7$ calcd 499.2444 found 499.2441.

*4.1.9.12. (S)-7-methoxy-8-((6-(3,4,5-trimethoxyphenoxy)hexyl)oxy)-1,2,3,11a-tetrahydro-5H-benzo[e]pyrrolo[1,2-a][1,4]diazepin-5-one (**5d**).* Light yellow oil; Yield: 79%; ^{1}H NMR ($CDCl_3$, 400 MHz) δ 7.67 (d, J = 4.4 Hz, 1H), 7.51 (s, 1H), 6.81 (s, 1H), 6.15 (s, 2H), 4.15–4.02 (m, 2H), 3.96 (t, J = 6.0 Hz, 2H), 3.95 (s, 3H), 3.86 (s, 6H), 3.79 (s, 3H), 3.78–3.55 (m, 3H), 3.48 (s, 1H), 2.36–2.30 (m, 2H), 2.10–1.80 (m, 6H), 1.57–1.54 (m, 3H); ^{13}C NMR ($CDCl_3$, 100 MHz) δ 164.6, 162.3, 155.7, 153.6, 150.8, 147.7, 140.6, 132.1, 120.1, 111.5, 110.4, 92.2, 68.8, 68.1, 60.9, 56.1, 56.0, 53.7, 46.6, 29.6, 29.2, 28.8, 25.8, 25.7, 24.1; HRMS (ESI, m/z) $C_{28}H_{36}N_2O_7$ calcd 512.6030 found 512.6031.

*4.1.9.13. N-(4-hydroxybutyl)-3,4,5-trimethoxybenzamide (**8b**).* Pale yellow solid; Yield: 97%; ^{1}H NMR ($CDCl_3$, 400 MHz) δ 7.03 (s, 2H), 6.86–6.83 (m, 1H), 3.88 (s, 6H), 3.87 (s, 3H), 3.71 (t, J = 6.0 Hz,

2H), 3.45 (q, J = 6.0 Hz, 2H), 2.53–2.01 (s, 1H), 1.75–1.64 (m, 4H); ^{13}C NMR ($CDCl_3$, 100 MHz) δ 167.4, 153.1, 140.7, 130.1, 104.3, 62.3, 60.8, 56.2, 39.9, 29.8, 26.2; HRMS (ESI, m/z) $C_{14}H_{21}NO_5Na$ calcd 306.1317 found 306.1316.

*4.1.9.14. N-(5-hydroxypentyl)-3,4,5-trimethoxybenzamide (**8c**).* Pale yellow solid; Yield: 95%; ^{1}H NMR ($CDCl_3$, 400 MHz) δ 7.17–7.14 (m, 1H), 7.07 (s, 2H), 3.85 (s, 6H), 3.84 (s, 3H), 3.59 (t, J = 6.0 Hz, 2H), 3.39 (q, J = 6.0 Hz, 2H), 3.32–3.01 (s, 1H), 1.62–1.51 (m, 4H), 1.43–1.37 (m, 2H); ^{13}C NMR ($CDCl_3$, 100 MHz) δ 167.3, 152.8, 140.4, 129.9, 104.3, 62.0, 60.6, 55.9, 39.9, 31.9, 29.0, 22.9; HRMS (ESI, m/z) $C_{15}H_{23}NO_5Na$ calcd 320.1474 found 320.1471.

*4.1.9.15. N-(6-hydroxyhexyl)-3,4,5-trimethoxybenzamide (**8d**).* Pale yellow solid; Yield: 93%; ^{1}H NMR ($CDCl_3$, 400 MHz) δ 7.03 (s, 2H), 6.59–6.58 (m, 1H), 3.88 (s, 6H), 3.87 (s, 3H), 3.61 (t, J = 6.0 Hz, 2H), 3.44 (q, J = 6.0 Hz, 2H), 2.28–2.25 (s, 1H), 1.64–1.51 (m, 4H), 1.39–1.34 (m, 4H); ^{13}C NMR ($CDCl_3$, 100 MHz) δ 167.2, 152.9, 140.4, 129.9, 104.1, 62.3, 60.7, 56.0, 39.8, 32.2, 29.4, 26.3, 25.1; HRMS (ESI, m/z) $C_{16}H_{25}NO_5Na$ calcd 334.1630 found 306.1633.

*4.1.9.16. 4-(3,4,5-trimethoxybenzamido)butyl 4-methylbenzenesulfonate (**9b**).* White solid; Yield: 66%; ^{1}H NMR ($CDCl_3$, 400 MHz) δ 7.74 (d, J = 4.4 Hz, 2H), 7.34 (d, J = 4.4 Hz, 2H), δ 7.08 (s, 2H), 7.06–7.03 (m, 1H), 4.03 (t, J = 6.0 Hz, 2H), 3.86 (s, 6H), 3.85 (s, 3H), 3.39 (q, J = 6.0 Hz, 2H), 2.43 (s, 3H), 1.74–1.60 (m, 4H); ^{13}C NMR ($CDCl_3$, 100 MHz) δ 167.1, 152.8, 144.8, 140.3, 132.4, 129.7, 129.6, 127.5, 104.1, 70.2, 60.6, 55.9, 39.0, 26.1, 25.4, 21.4, HRMS (ESI, m/z) $C_{21}H_{27}NO_7SNa$ calcd 460.1406 found 460.1408.

*4.1.9.17. 5-(3,4,5-trimethoxybenzamido)pentyl 4-methylbenzenesulfonate (**9c**).* White solid; Yield: 70%; ^{1}H NMR ($CDCl_3$, 400 MHz) δ 7.75 (d, J = 4.4 Hz, 2H), 7.35 (d, J = 4.4 Hz, 2H), 7.32–7.29 (m, 1H), 7.13 (s, 2H), 3.99 (t, J = 6.0 Hz, 2H), 3.85 (s, 6H), 3.83 (s, 3H), 3.37 (q, J = 6.0 Hz, 2H), 2.43 (s, 3H), 1.68–1.34 (m, 6H); ^{13}C NMR ($CDCl_3$, 100 MHz) δ 166.8, 152.5, 144.6, 140.0, 132.3, 129.6, 129.5, 127.3, 104.0, 70.2, 60.3, 55.7, 39.4, 28.4, 28.0, 22.3, 21.1; HRMS (ESI, m/z) $C_{22}H_{29}NO_7SNa$ calcd 474.1562 found 474.1560.

*4.1.9.18. 6-(3,4,5-trimethoxybenzamido)hexyl 4-methylbenzenesulfonate (**9d**).* White solid; Yield: 61%; ^{1}H NMR ($CDCl_3$, 400 MHz) δ 7.77 (d, J = 4.4 Hz, 2H), 7.33 (d, J = 4.4 Hz, 2H), 7.05 (s, 2H), 6.67–6.64 (m, 1H), 4.02 (t, J = 7.2 Hz, 2H), 3.87 (s, 6H), 3.86 (s, 3H), 3.42–3.34 (m, 2H), 2.45 (s, 3H), 1.66–1.23 (m, 8H); ^{13}C NMR ($CDCl_3$, 100 MHz) δ 167.1, 152.9, 144.7, 140.4, 132.7, 129.8, 129.5, 127.6, 104.2, 70.4, 60.7, 56.1, 39.8, 29.2, 28.5, 25.9, 24.8, 21.5; HRMS (ESI, m/z) $C_{23}H_{31}NO_7SNa$ calcd 488.1819 found 488.1721.

*4.1.9.19. (S)-N-(4-((10-(ethoxymethyl)-7-methoxy-5,11-dioxo-2,3,5,10,11,11a-hexahydro-1H-benzo[e]pyrrolo[1,2-a][1,4]diazepin-8-yl)oxy)butyl)-3,4,5-trimethoxybenzamide (**10b**).* Light yellow oil; Yield: 80%; ^{1}H NMR ($CDCl_3$, 400 MHz) δ 7.33 (s, 1H), 7.25 (s, 1H), 7.21–7.18 (m, 1H), 7.11 (s, 2H), 5.57 (d, J = 10.0 Hz, 1H), 4.67 (d, J = 10.0 Hz, 1H), 4.16–4.05 (m, 3H), 3.87 (s, 3H), 3.86 (s, 6H), 3.81 (s,3H), 3.80–3.65 (m, 2H), 3.65–3.50 (m, 4H), 2.74–2.70 (m, 1H), 2.11–1.94 (m, 5H), 1.88–1.83 (m, 2H), 1.28 (t, J = 7.2 Hz, 3H); ^{13}C NMR ($CDCl_3$, 100 MHz) δ 170.0, 167.0, 164.9, 152.8, 150.7, 146.7, 140.4, 133.8, 129.9, 121.8, 110.9, 106.1, 104.2, 77.9, 68.5, 64.6, 60.6, 57.3, 55.9, 55.7, 46.5, 39.1, 26.3, 26.1, 25.7, 23.5, 15.1.

*4.1.9.20. (S)-N-(5-((10-(ethoxymethyl)-7-methoxy-5,11-dioxo-2,3,5,10,11,11a-hexahydro-1H-benzo[e]pyrrolo[1,2-a][1,4]diazepin-8-yl)oxy)pentyl)-3,4,5-trimethoxybenzamide (**10c**).* Light yellow oil; Yield: 81%; ^{1}H NMR ($CDCl_3$, 400 MHz) δ 7.32 (s, 1H), 7.23 (s, 1H), 7.07 (s, 2H), 6.8–6.87 (m, 1H), 5.57 (d, J = 10.0 Hz, 1H), 4.67 (d, J = 10.0 Hz, 1H), 4.15–4.01 (m, 3H), 3.86 (s, 3H), 3.85 (s, 6H), 3.84 (s,3H), 3.79–3.72 (m, 2H), 3.71–3.52 (m, 2H), 3.48–3.45 (m, 2H), 2.73–2.69 (m, 1H), 2.13–1.99 (m, 3H), 1.98–1.87 (m, 2H), 1.73–1.66 (m, 2H), 1.61–1.53 (m, 2H), 1.26 (t, J = 7.2 Hz, 3H); ^{13}C NMR ($CDCl_3$, 100 MHz) δ 170.1, 167.0, 164.9, 152.8, 150.9, 146.9, 140.4, 133.7, 129.9, 121.7, 111.1, 106.3, 104.2, 77.9, 68.7, 64.6, 60.6, 57.3, 55.9, 55.8, 46.5, 39.8, 29.1, 28.3, 26.3, 23.5, 23.4, 15.1; HRMS (ESI, m/z) $C_{31}H_{41}N_3O_9Na$ calcd 622.2740 found 622.2736.

*4.1.9.21. (S)-N-(6-((10-(ethoxymethyl)-7-methoxy-5,11-dioxo-2,3,5,10,11,11a-hexahydro-1H-benzo[e]pyrrolo[1,2-a][1,4]diazepin-8-yl)oxy)hexyl)-3,4,5-trimethoxybenzamide (**10d**).* Light yellow oil; Yield: 78%; ^{1}H NMR ($CDCl_3$, 400 MHz) δ 7.34 (s, 1H), 7.24 (s, 1H), 7.02 (s, 2H), 6.47–6.44 (m, 1H), 5.57 (d, J = 10.0 Hz, 1H), 4.67 (d, J = 10.0 Hz, 1H), 4.13–4.03 (m, 3H), 3.90 (s, 3H), 3.88 (s, 6H), 3.87 (s,3H), 3.76–3.73 (m, 2H), 3.65–3.52 (m, 2H), 3.44–3.43 (m, 2H), 2.73–2.69 (m, 1H), 2.13–1.98 (m, 3H), 1.91–1.84 (m, 2H), 1.69–1.62 (m, 2H), 1.57–1.43 (m, 4H), 1.28 (t, J = 7.2 Hz, 3H); ^{13}C NMR ($CDCl_3$, 100 MHz) δ 170.2, 167.1, 165.1, 153.0, 151.1, 147.1, 133.8, 130.1, 121.8, 111.2, 106.4, 104.2, 78.1, 68.8, 64.7, 60.8, 57.5, 56.2, 55.9, 46.6, 39.9, 29.6, 29.5, 28.6, 26.6, 26.4, 25.5, 23.6, 15.2; HRMS (ESI, m/z) $C_{32}H_{43}N_3O_9Na$ calcd 636.2900 found 636.2903.

*4.1.9.22. (S)-3,4,5-trimethoxy-N-(4-((7-methoxy-5-oxo-2,3,5,11a-tetrahydro-1H-benzo[e]pyrrolo[1,2-a][1,4]diazepin-8-yl)oxy)butyl) benzamide (**11b**).* Light yellow oil; Yield: 74%; ^{1}H NMR ($CDCl_3$, 400 MHz) δ 7.68 (d, J = 4.4 Hz, 1H), 7.51 (s, 1H), 7.07 (s, 2H), 6.88–6.86 (m, 1H), 6.81 (s, 1H), 4.20–4.08 (m, 2H), 3.88 (s, 3H), 3.87 (s, 6H), 3.81 (s, 3H), 3.75–3.66 (m, 2H), 3.62–3.49 (m, 3H), 2.36–2.31 (m, 2H), 2.12–1.96 (m, 4H), 1.90–1.82 (m, 2H); ^{13}C NMR ($CDCl_3$, 100 MHz) δ 167.2, 164.5, 162.6, 153.0, 150.1, 147.5, 140.7, 130.3, 120.3, 111.5, 110.2, 104.3, 68.7, 60.9, 56.2, 55.9, 53.7, 46.7, 39.2, 29.6, 26.5, 25.8, 24.2; HRMS (ESI, m/z) $C_{27}H_{33}N_3O_7$ calcd 512.2397 found 512.2401.

*4.1.9.23. (S)-3,4,5-trimethoxy-N-(5-((7-methoxy-5-oxo-2,3,5,11a-tetrahydro-1H-benzo[e]pyrrolo[1,2-a][1,4]diazepin-8-yl)oxy)pentyl) benzamide (**11c**).* Light yellow oil; Yield: 73%; ^{1}H NMR ($CDCl_3$, 400 MHz) δ 7.67 (d, J = 4.4 Hz, 1H), 7.49 (s, 1H), 7.04 (s, 2H), 6.79 (s, 1H), 6.57–6.56 (m, 1H), 4.11–4.02 (m, 2H), 3.88 (s, 3H), 3.87 (s, 6H), 3.81 (s, 3H), 3.75–3.66 (m, 2H), 3.62–3.44 (m, 3H), 2.34–2.29 (m, 2H), 2.09–2.88 (m, 6H), 1.73–1.50 (m, 2H); ^{13}C NMR ($CDCl_3$, 100 MHz) δ 167.2, 164.8, 162.8, 153.3, 150.9, 147.9, 140.8, 130.4, 120.4, 111.7, 110.6, 104.5, 69.1, 61.1, 56.5, 56.3, 53.9, 46.9, 40.3, 29.8, 29.4, 28.7, 24.4, 23.9; HRMS (ESI, m/z) $C_{28}H_{35}N_3O_7$ calcd 526.2553 found 526.2555.

*4.1.9.24. (S)-3,4,5-trimethoxy-N-(6-((7-methoxy-5-oxo-2,3,5,11a-tetrahydro-1H-benzo[e]pyrrolo[1,2-a][1,4]diazepin-8-yl)oxy)hexyl) benzamide (**11d**).* Light yellow oil; Yield: 77%; ^{1}H NMR ($CDCl_3$, 400 MHz) δ 7.67 (d, J = 4.4 Hz, 1H), 7.51 (s, 1H), 7.00 (s, 2H), 6.79 (s, 1H), 6.26–6.22 (m, 1H), 4.11–4.05 (m, 2H), 3.93 (s, 3H), 3.91 (s, 6H), 3.88 (s, 3H), 3.81–3.73 (m, 2H), 3.62–3.44 (m, 3H), 2.36–2.29 (m, 2H), 2.07–1.87 (m, 4H), 1.66–1.24 (m, 6H); ^{13}C NMR ($CDCl_3$, 100 MHz) δ 167.3, 164.6, 162.4, 153.2, 150.8, 147.8, 140.6, 130.3, 120.1, 111.5, 110.4, 104.3, 68.8, 60.9, 56.3, 56.1, 53.7, 46.7, 40.1, 29.7, 29.6, 28.7, 26.6, 25.6, 24.2; HRMS (ESI, m/z) $C_{29}H_{37}N_3O_7$ calcd 540.2710 found 540.2711.

4.2. Experimental protocol for biological studies

4.2.1. Cell culture

Compounds were dissolved in DMSO at a final concentration of 10 mM and store at −20 °C. Several cell lines, human melanoma (A375 and RPMI7951), breast (MCF-7), lung (A549, H1299), and

mouse melanoma (B16) purchased from American Type Culture Collection (Manassas, VA), was maintained in DMEM (A375, B16), MEM (RPMI7951, MCF-7), RPMI1640 (A549) or DMEM-F12 (H1299) supplemented with10% FCS and 100 U/mL penicillin G, and 100 μg/mL streptomycin sulfate (Gibco, BRL). Cells were passaged at confluence after treatment with 5 mM EDTA (Gibco, BRL) and incubated at 37 °C in a humidified atmosphere containing 5% CO_2. Fibroblasts were obtained from adult foreskin specimens as previously described.[53].

4.2.2. Cell viability

The protocols used were as described previously [7].

4.2.3. Colony formation assay

A375 cells were plated into 6-well plates at a density of 100 cells per well. On the second day, cells were treated with PBD-GA. Every 3 days, the medium was replaced with fresh medium containing the agent at 0.5 μM concentration. After a 10 day treatment, the medium was removed, and cell colonies were stained with SRB dyes, and pictures were taken using a digital camera.

4.2.4. Determination of intracellular ROS level

The methods used were as reported previously [8].

4.2.5. Mitochondrial membrane potential assessment ($\Delta\Psi_{mt}$)

The methods utilized were as described previously [8].

4.2.6. Immunocytochemical staining

To clarify the role of the DNA damage indicator p-ATR and p-ATM, the 8-oxoguanine oxidative stress marker, the mitochondrial marker COX IV and cytochrome c in A375 cells; cathespin D and LAMP-1 in RPMI7951 cells; tumor apoptosis marker Annexin V/PI in B16 cells treated with PBD-GA and its expression were correlated with apoptotic. Cells were seeded on glass coverslips with a density of 1×10^4 cells and were incubated overnight. The cells were treated with 0.5 μM PBD-GA for 24 h. Immunocytochemistry was performed on all test samples. Cells were washed several times by using PBS and fix by 4% formaldehyde for 5 min at 4 °C, then permeabilized cell with 0.5% Triton X-100 for 5 min. Non-specific binding was blocked by 5% bovine serum albumin at 37 °C for 45 min. Cells were incubated 1 h with primary antibodies (mouse anti-p-ATR and mouse anti-p-ATM at 1:1000, mouse anti-8-oxoguanine 1:250, rabbit anti-COX IV and mouse anti-cytochrome c at 1:1000, mouse anti-LAMP1 and rabbit anti-cathepsin D at 1:500) at RT. Subsequently, slides were incubated with secondary antibodies for 30 min at RT. Finally, added about 40 μL mounting medium contains DAPI to slide and cover with glass coverslips then sealed with nail polish.

4.2.7. Cell cycle analysis

The methods used were as reported previously [7].

4.2.8. Quantitative RT-PCR

The methods used were as reported previously [7].

The primers used were:

p53: forward, 5′-CCATCCACTACAACTACATGTG - 3′; reverse, 5′ - AAAGCTGTTCCGTCCCAGTA - 3′
bax: forward, 5′- GGATGCGTCCACCACCAAGAAG - 3′; reverse, 5′ - GCCTTGAGCACCAGTTTGC - 3′
bcl-xl: forward, 5′- GCACTGTGCGTGGAAAGCGTAGAC - 3′; reverse, 5′ - CTGAAGAGTGAGCCCAGCAGAACC - 3′
GAPDH: forward, 5′ - GAAGGTGAAGGTCGGAGTCAACG - 3′; reverse, 5′ - AGTCCTTCCACGATAACCAAAGTTG - 3′

4.2.9. Gene knockdown

A375 cell was plated in 12-well plates at 6×10^4 cells per well and cultured overnight at 37 °C in 1 mL of DMEM medium without antibiotics. The next day, each well was transfected with 30 nM siRNA specific for tp53 with 1.5 μL of Lipofectamine RNAiMAX (Invitrogen). Transfection with 30 nM non target siRNA with 1.5 μL of Lipofectamine served as the negative control. Cells were harvested 24 h after siRNA transfection and then subjected to analyses.

4.2.10. p53 siRNA

forward, 5′- UUACACAUGUAGUUGUAGUGGAUG - 3′; reverse, 5′ - CCAUCCACUACAACUACAUGUGUA - 3′

4.2.11. Lysosomal H^+ measurement

RPMI 7951 cells were incubated with LysoTracker Green (75 nM) for 15 min at 37 °C prior to treatment with compounds for indicated times. Cells were washed and mean fluorescence quantified with flow cytometer.

4.2.12. Protein extraction and western blot analysis

Mouse monoclonal antibody against p53 and Cdc25c were purchased from Santa Cruz Biotechnology (Santa Cruz, CA, USA). Rabbit polyclonal antibody against p-p53, p-Chk1, BCL-XL and PARP were purchased from Cell Signaling Biotechnology (Boston, MA, USA), GeneTex (Irvine, CA, USA), ABGENT (Sandiego, CA, USA) and Santa Cruz Biotechnology (Santa Cruz, CA, USA), respectively. Mouse monoclonal antibody against GAPDH and caspase-3 were purchased from GeneTex (Irvine, CA, USA) and ABGENT (Sandiego, CA, USA). The methods used were as reported previously [54].

4.2.13. Annexin V/PI staining

Cultured B16 cells were seeded on glass coverslips with a density of 3×10^5 cells/well in 6-well plate for 24 h until cell attachment. Then the cells were exposed to compounds at 0.5 μM for 24 h. The cells were washed twice with PBS and were then stained with annexin V- FITC and PI (Annexin V-FITC Apoptosis detection Kit; Strong Biotech Corporation, Taiwan), and then incubated at room temperature for at least 15 min in the dark. After staining, the preparations were washed and transferred to glass slides for observation under a fluorescence microscope (Leica DMI6000, Wetzlar Germany).

4.2.14. Animal experiment

Seven-week-old female ICR strain mice were obtained and maintained as described in our previous study.54 B16 cells were harvested from in vitro incubation and were inoculated s.c. at 1×10^6 per animal in 20 μl PBS into the footpad of ICR mice. When tumors had reached a mean diameter of 4–7 mm (day 0), the animals were randomized into groups of three and treated by i.v. injection at 0, 2, 4 mg/kg. Body weights and two perpendicular diameters of the tumors were measured at least 3 times per week. Each tumor volume was calculated according to the following equation: $v = 0.5236[(l + w)/2]^3$, where l and w are the largest and smallest perpendicular diameters. Tumor volume and body weights were expressed as mean ± SEM relative to tumor volume or body weight values on day 0 (start of treatment). The T/C% ratio (mean relative tumor volume of the treated tumors/mean relative volume of control group = 100) was calculated each time the tumors were measured. The lowest value is expressed as the optimal T/C% for each group. Statistical analysis was performed using t-test.

4.2.15. Statistical analysis

The methods used were as reported previously [7].

Acknowledgment

We gratefully acknowledge funding from the Ministry of Science and Technology (MOST), Taiwan. Also supported by a grant from the Kaohsiung Medical University Research Foundation (KMU-M102001).

Appendix A. Supporting information

Supporting information related to this article can be found at http://dx.doi.org/10.1016/j.ejmech.2015.12.039.

Experimental procedures for QSAR studies and docking figures for compound **5a**,**d** and **11a**–**d**. ^{1}H and ^{13}C spectra for the compounds **2**, **4**, **5**, **8**, **9**, **10** and **11**. The HPLC chromatogram for the compounds **5a**–**d** and **11a**–**d**.

References

[1] D.E. Thurston, Advances in the study of pyrrolo[2,1-c][1, 4]-benzodiazepine (PBD) antitumor antibiotics, in: S. Neidle, M.J. Waring (Eds.), Molecular Aspects of Anticancer Drug-DNA Interactions, vol. 1, Macmillan Press, New York, 1993, p. 54.
[2] S. Alcaro, F. Ortuso, R.S. Coleman, DNA cross-linking by azinomycin B: Monte Carlo simulations in the evaluation of sequence selectivity, J. Med. Chem. 45 (2002) 861–865.
[3] M. Rettig, W. Langel, A. Kamal, K. Weisz, NMR structural studies on the covalent DNA binding of a pyrrolobenzodiazepine–naphthalimide conjugate, Org. Biomol. Chem. 8 (2010) 3179–3187.
[4] W.–P. Hu, J.–J. Wang, F.L. Lin, Y.C. Lin, S.R. Lin, M.H. Hsu, An efficient synthesis of pyrrolo[2,1-c]-[1,4]benzodiazepine. Synthesis of the antibiotic DC-81, J. Org. Chem. 66 (2001) 2881–2883.
[5] P.E. Cross, R.P. Dickinson, M.J. Parry, M.J. Randall, Selective thromboxane synthetase inhibitors. 3. 1H-imidazol-1-yl-substituted benzo[b]furan-, benzo [b]thiophene-, and indole-2- and -3-carboxylic acids, J. Med. Chem. 29 (1986) 1637–1643.
[6] S. Mahboobi, H. Pongratz, H. Hufsky, J. Hockemeyer, M. Frieser, A. Lyssenko, D.H. Paper, J. Bürgermeister, F.D. Böhmer, H.H. Fiebig, A.M. Burger, S. Baasner, T. Beckers, Synthetic 2-aroylindole derivatives as a new class of potent tubulin-inhibitory, antimitotic agents, J. Med. Chem. 44 (2001) 4535–4553.
[7] J.J. Wang, Y.K. Shen, W.P. Hu, M.C. Hsieh, F.L. Lin, M.K. Hsu, M.H. Hsu, Design, synthesis, and biological evaluation of pyrrolo[2,1-c][1,4]benzodiazepine and indole conjugates as anticancer agents, J. Med. Chem. 49 (2006) 1442–1449.
[8] W.P. Hu, H.S. Yu, P.J. Sung, F.Y. Tsai, Y.K. Shen, L.S. Chang, J.J. Wang, DC-81-indole conjugate agent induces mitochondria mediated apoptosis in human melanoma A375 cells, Chem. Res. Toxicol. 20 (2007) 905–912.
[9] W.P. Hu, F.Y. Tsai, H.S. Yu, P.J. Sung, L.S. Chang, J.J. Wang, Induction of apoptosis by DC-81-indole conjugate agent through NF-kappaB and JNK/AP-1 pathway, Chem. Res. Toxicol. 21 (2008) 1330–1336.
[10] C.H. Lee, W.P. Hu, C.H. Hong, H.S. Yu, W.T. Liao, C.Y. Chen, Y.L. Chen, B.H. Chen, G.S. Chen, J.J. Wang, Pyrrolo[2,1-c][1,4]benzodiazepine and indole conjugate (IN6CPBD) has better efficacy and superior safety than the mother compound DC-81 in suppressing the growth of established melanoma in vivo, Chem. Biol. Interact. 180 (2009) 360–367.
[11] M.C. Hsieh, W.P. Hu, H.S. Yu, W.C. Wu, L.S. Chang, Y.H. Kao, J.J. Wang, A DC 81-indole conjugate agent suppresses melanoma A375 cell migration partially via interrupting VEGF production and stromal cell-derived factor-1α-mediated signaling, Toxicol. Appl. Pharmacol. 150 (2011) 150–159.
[12] M. Konishi, H. Ohkuma, T. Tsuno, T. Oki, G.D. VanDuyne, J. Clardy, Crystal and molecular structure of dynemicin A: a novel 1,5-diyn-3-ene antitumor antibiotic, J. Am. Chem. Soc. 112 (1990) 3715–3716.
[13] M.D. Lee, T.S. Dunne, M.M. Siegel, C.C. Chang, G.O. Morton, D.B. Borders, Calichemicins, a novel family of antitumor antibiotics. 1. Chemistry and partial structure of calichemicin.gamma.1I, J. Am. Chem. Soc. 109 (1987) 3464–3466.
[14] K.C. Nicolaou, W.M. Dai, Chemistry and biology of the enediyne anticancer antibiotics, Angew. Chem. Int. Ed. 30 (1991) 1387–1416.
[15] W.P. Hu, J.J. Liang, C.L. Kao, Y.C. Chen, C.Y. Chen, F.Y. Tsai, M.J. Wu, L.S. Chang, Y.L. Chen, J.J. Wang, Synthesis and antitumor activity of novel enediyne -linked pyrrolo[2,1-c] [1,4]benzodiazepine hybrids, Bioorg. Med. Chem. 17 (2009) 1172–1180.
[16] C.Y. Chen, Y.K. Chen, J.J. Wang, C.C. Hsu, F.Y. Tsai, P.J. Sung, H.C. Lin, L.S. Hu, W.P. Chang, DC-81-enediyne induces apoptosis of human melanoma A375 cells: involvement of the ROS, p38 MAPK, and AP-1 signaling pathways, Cell. Biol. Toxicol. 29 (2013) 85–99.
[17] H. Khaledi, A.A. Alhadi, W.A. Yehye, H.M. Ali, M.A. Abdulla, P. Hassandarvish, Antioxidant, cytotoxic activities, and structure–activity relationship of gallic acid-based indole derivatives, Arch. Pharm. Chem. Life Sci. 344 (2011) 703–709.
[18] M. Uozaki, H. Yamasaki, Y. Katsuyama, M. Higuchi, T. Higuti, A.H. Koyama, Antiviral effect of octyl gallate against DNA and RNA viruses, Antivir. Res. 73 (2007) 85–91.
[19] A. Bernhaus, M. Fritzer-Szekeres, M. Grusch, P. Saiko, G. Krupitza, S. Venkateswarlu, G. Trimurtulu, W. Jaeger, T. Szekeres, Digalloylresveratrol, a new phenolic acid derivative induces apoptosis and cell cycle arrest in human HT-29 colon cancer cells, Cancer Lett. 274 (2009) 299–304.
[20] J.A. Jara, V. Castro-Castillo, J. Saavedra-Olavarría, L. Peredo, M. Pavanni, F. Jaña, M.E. Letelier, E. Parra, M.I. Becker, A. Morello, U. Kemmerling, J.D. Maya, J. Ferreira, Antiproliferative and uncoupling effects of delocalized, lipophilic, cationic gallic acid derivatives on cancer cell lines. Validation in vivo in singenic mice, J. Med. Chem. 57 (2014) 2440–2454.
[21] M. Inoue, R. Suzuki, T. Koide, N. Sakaguchi, Y. Ogihara, Y. Yabu, Antioxidant, gallic acid, induces apoptosis in HL-60RG cells, Biochem. Biophys. Res. Commun. 204 (1994) 898–904.
[22] H.M. Chen, Y.C. Wu, Y.C. Chia, F.R. Chang, H.K. Hsu, Y.C. Hsieh, C.C. Chen, S.S. Yuan, Gallic acid, a major component of Toona sinensis leaf extracts, contains a ROS-mediated anti-cancer activity in human prostate cancer cells, Cancer Lett. 286 (2009) 161–171.
[23] J. Wang, J. Yi, Cancer cell killing via ROS: to increase or decrease that is the question, Cancer Biol. Ther. 7 (2008) 1875–1884.
[24] D. Trachootham, Y. Zhou, H. Zhang, Y. Demizu, Z. Chen, H. Pelicano, P.J. Chiao, G. Achanta, R.B. Arlinghaus, J. Liu, P. Huang, Selective killing of oncogenically transformed cells through a ROS-mediated mechanism by beta-phenylethyl isothiocyanate, Cancer Cell 10 (2006) 241–252.
[25] M. Crompton, The mitochondrial permeability transition pore and its role in cell death, Biochem. J. 341 (1999) 233–249.
[26] D. Dominguez-Sola, C.Y. Ying, C. Grandori, L. Ruggiero, B. Chen, M. Li, D.A. Galloway, W. Gu, J. Gautier, R. Dalla-Faver, Non-transcriptional control of DNA replication by c-Myc, Nature 448 (2007) 445–451.
[27] B. Fadeel, S. Orrenius, Apoptosis: a basic biological phenomenon with wide-ranging implications in human disease, J. Intern Med. 258 (2005) 479–517.
[28] C. de Duve, Lysosomes revisited, Eur. J. Biochem. 137 (1983) 391–397.
[29] B. Turk, V. Stoka, Protease signalling in cell death: caspases versus cysteine cathepsins, FEBS Lett. 581 (2007) 2761.
[30] A. Kamal, R.V.C.R.N.C. Shetti, M.J. Ramaiah, P. Swapna, K.S. Reddy, A. Mallareddy, M.P.N. Rao, M. Chourasia, G.N. Sastry, A. Juvekar, S. Zingde, P. Sarma, S.N.C.V.L. Pushpavalli, M.P. Bhadra, Carbazole–pyrrolo[2,1-c][1,4] benzodiazepine conjugates: design, synthesis, and biological evaluation, Med. Chem. Commun. 2 (2011) 780–788.
[31] R.X. Xu, A.M. Hassell, D. Vanderwall, M.H. Lambert, W.D. Holmes, M.A. Luther, W.J. Rocque, M.V. Milburn, Y. Zhao, H. Ke, R.T. Nolte, Atomic structure of PDE4: insights into phosphodiesterase mechanism and specificity, Science 288 (2000) 1822–1825.
[32] A. Kamal, M.K. Reddy, A.K. Srivastava, Y.V.V. Srikanth, (2012) Pyrrolobenzodiazepines as Sequence Selective DNA Binding Agents, Medicinal Chemistry and Drug Design, Prof Deniz Ekinci (Ed.), ISBN: 978-953-51-0513-8, InTech, Available from: intechopen.com/books/medicinal-chemistry-and drug-design/pyrrolobenzodiazepines-as-sequence-selective-dna-binding-agents.
[33] A. Barzilai, K. Yamamoto, DNA damage responses to oxidative stress, DNA Repair 3 (2004) 1109–1115.
[34] W. Meikrantz, R. Schlegel, Apoptosis and the cell cycle, J. Cell Biochem. 58 (1995) 160–174.
[35] M.B. Kastan, D.S. Lim, The many substrates and functions of ATM, Nat. Rev. Mol. Cell. Biol. 1 (2000) 179–186.
[36] N. Rhind, P. Russell, Chk1 and Cds1: linchpins of the DNA damage and replication checkpoint pathways, J. Cell Sci. 113 (2000) 3889–3896.
[37] J. Bartek, J. Lukas, Chk1 and Chk2 kinases in checkpoint control and cancer, Cancer Cell 3 (2003) 421–429.
[38] J. Hutson, J. Ramsdale, M. Wells, p53 protein expression in putative precursor lesions of epithelial ovarian cancer, Histopathology 27 (1995) 367–371.
[39] C.K. Ho, G. Li, Mutant p53 melanoma cell lines respond differently to CP-31398-induced apoptosis, Br. J. Dermatol. 153 (2005) 900–910.
[40] G.S. Salvesen, V.M. Dixit, Caspases: intracellular signaling by proteolysis, Cell 91 (1997) 443–448.
[41] Y. Shi, Mechanisms of caspase activation and inhibition during apoptosis, Mol. Cell. 9 (2002) 459–470.
[42] D.A. Hildeman, T. Mitchell, T.K. Teague, P. Henson, B.J. Day, J. Kappler, P.C. Marrack, Reactive oxygen species regulate activation-induced T cell apoptosis, Immunity 10 (1999) 735–744.
[43] C.C. Yang, S.D. Lin, H.S. Yu, Effect of growth factors on dermal fibroblast contraction in normal skin and hypertrophic scar, J. Dermatol. Sci. 14 (1997) 162–169.
[44] R.M. Kluck, E. Bossy-Wetzel, D.R. Green, D.D. Newmeyer, The release of cytochrome c from mitochondria: a primary site for Bcl-2 regulation of apoptosis, Science 275 (1997) 1132–1136.
[45] E. Rudolf, M. Cervinka, Sulforaphane induces cytotoxicity and lysosome- and mitochondria-dependent cell death in colon cancer cells with deleted p53, Toxicol Vitro 25 (2011) 1302–1309.
[46] P. Boya, Lysosomal function and dysfunction: mechanism and disease, Antioxid. Redox Signal 17 (2012) 766–774.
[47] C.E. Chwieralski, T. Welte, F. Bühling, Cathepsin-regulated apoptosis,

Apoptosis 11 (2006) 143–149.
[48] A.C. Johansson, H. Appelqvist, C. Nilsson, K. Kågedal, K. Roberg, K. Ollinger, Regulation of apoptosis-associated lysosomal membrane permeabilization, Apoptosis 15 (2010) 527–540.
[49] S. Pervaiz, M.A. Seyed, J.L. Hirpara, M.V. Clément, K.W. Loh, Purified photoproducts of merocyanine 540 trigger cytochrome C release and caspase 8-dependent apoptosis in human leukemia and melanoma cells, Blood 93 (1999) 4096–4108.